COROTATING INTERACTION REGIONS AT HIGH LATITUDES

Report of Working Group 3

H. KUNOW[1] AND M. A. LEE[2]
CO-CHAIRS

L. A. FISK[3], R. J. FORSYTH[4], B. HEBER[5], T. S. HORBURY[4,6], E. KEPPLER[5], J. KÓTA[7], Y.-Q. LOU[9], R. B. MCKIBBEN[8], C. PAIZIS[9], M. S. POTGIETER[10], E. C. ROELOF[11], T. R. SANDERSON[12], G. M. SIMNETT[13], R. VON STEIGER[14], B. T. TSURUTANI[15], AND R. F. WIMMER-SCHWEINGRUBER[16]
PARTICIPANTS

J. R. JOKIPII[7]
CONTRIBUTING AUTHOR NOT PARTICIPATING IN THE WORKING GROUP

[1]*Extraterrestrische Physik, Universität Kiel, Kiel, Germany*
[2]*Space Science Center, University of New Hampshire, Durham, New Hampshire, USA*
[3]*Dept. of Atmospheric and Space Sciences, University of Michigan, Ann Arbor, Michigan, USA*
[4]*The Blackett Laboratory, Imperial College, London, United Kingdom*
[5]*Max-Planck-Institut für Aeronomie, Katlenburg-Lindau, Germany*
[6]*now at Queen Mary and Westfield College, London, United Kingdom*
[7]*Depts. of Planetary Sciences and Astronomy, University of Arizona, Tucson, Arizona, USA*
[8]*Enrico Fermi Institute, University of Chicago, Chicago, Illinois, USA*
[9]*Dipartimento di Fisica, Università di Milano, Milano, Italy*
[10]*Potchefstroom University for CHE, Potchefstroom, South Africa*
[11]*Applied Physics Laboratory, Johns Hopkins University, Laurel, Maryland, USA*
[12]*Space Science Dept., ESA/ESTEC, Noordwijk, The Netherlands*
[13]*Physics and Astronomy Dept., University of Birmingham, Birmingham, United Kingdom*
[14]*International Space Science Institute, Bern, Switzerland*
[15]*Jet Propulsion Laboratory, Pasadena, California, USA*
[16]*Physikalisches Institut der Universität Bern, Bern, Switzerland*

Received: 6 June 1999; Accepted: 8 July 1999

Abstract. Ulysses observed a stable strong CIR from early 1992 through 1994 during its first journey into the southern hemisphere. After the rapid latitude scan in early 1995, Ulysses observed a weaker CIR from early 1996 to mid-1997 in the northern hemisphere as it traveled back to the ecliptic at the orbit of Jupiter. These two CIRs are the observational basis of the investigation into the latitudinal structure of CIRs. The first CIR was caused by an extension of the northern coronal hole into the southern hemisphere during declining solar activity, whereas the second CIR near solar minimum activity was caused by small warps in the streamer belt. The latitudinal structure is described through the presentation of three 26-day periods during the southern CIR. The first at $\sim$24°S shows the full plasma interaction region including fast and slow wind streams, the compressed shocked flows with embedded stream interface and heliospheric current sheet (HCS), and the forward and reverse shocks with associated accelerated ions and electrons. The second at 40°S exhibits only the reverse shock, accelerated particles, and the 26-day modulation of cosmic rays. The third at 60°S shows only the accelerated particles and modulated cosmic rays. The possible mechanisms for the access of the accelerated particles and the CIR-modulated cosmic rays to high latitudes above the plasma

Space Science Reviews **89:** 221–268, 1999.

interaction region are presented. They include direct magnetic field connection across latitude due to stochastic field line weaving or to systematic weaving caused by solar differential rotation combined with non-radial expansion of the fast wind. Another possible mechanism is particle diffusion across the average magnetic field, which includes stochastic field line weaving. A constraint on connection to a distant portion of the CIR is energy loss in the solar wind, which is substantial for the relatively slow-moving accelerated ions. Finally, the weaker northern CIR is compared with the southern CIR. It is weak because the inclination of the streamer belt and HCS decreased as Ulysses traveled to lower latitudes so that the spacecraft remained at about the maximum latitudinal extent of the HCS.

Keywords: Solar wind, interplanetary medium, CIRs, high latitude heliosphere

1. Introduction

M. A. LEE and H. KUNOW

The origin of corotating interaction regions (CIRs) in the solar wind is to be found in the pattern of slow and fast solar wind accelerated at the Sun. Near solar minimum activity fast wind originates in polar coronal holes. Slow wind originates adjacent to or above active regions to create a 'streamer belt' of slow wind around the Sun evident in white-light coronagraph images. The coronal magnetic field channels the wind streams, which in turn draw the field into a radial configuration. At a 'source surface' about the Sun with a heliocentric radius of a few solar radii the solar wind consists of fast streams at higher heliographic latitudes separated by an irregular band of slow wind at lower latitudes. The wind is approximately radial, with embedded radial magnetic field, and in lateral pressure balance. The streamer belt encases the heliospheric current sheet (HCS), whose location on the source surface can be estimated by extrapolating from the observed photospheric magnetic field assuming that the field is a potential field and is radial at the source surface (Hoeksema *et al.*, 1982). As the Sun becomes more active the coronal holes shrink and the pattern of slow and fast wind becomes more irregular. Slow wind may ultimately dominate at solar maximum activity, resulting in a simpler underlying wind, but disturbed by frequent coronal mass ejections.

Because of solar rotation the stream interfaces and HCS on the source surface map into the heliosphere along a family of Archimedian spirals, neglecting for a moment the difference in the fast and slow wind speeds that results in two families of spirals. In simple cases the resulting surfaces may approximate the ballerina skirt popularized by Jokipii and Thomas (1981). An interaction region develops wherever the stream interface surface separates slow wind ahead of fast wind. With increasing heliocentric radial distance r, the fast wind then runs into the slow wind to create a compression region. Conversely, where slow wind trails fast wind, a rarefaction region develops. If the pattern of fast and slow wind at the source surface is stable over several solar rotations, then the interaction region is called a CIR since the configuration is approximately stationary in the frame which corotates with the Sun.

The nature and strength of the interaction is determined by the local unit normal to the interface **n** (see discussion in Sect. 3 of Crooker, Gosling *et al.*, 1999, in this volume). The compression is due to the component of the difference in the fast and slow wind velocities $\Delta V \mathbf{e_r}$ in the **n** direction, $\Delta V \mathbf{n} \cdot \mathbf{e_r}$, where $\mathbf{e_r}$ is the unit vector in the radial direction. The quantity $|\mathbf{n} \cdot \mathbf{e_r}|$ increases with r due to solar rotation and spherical expansion. The compression increases the radial speed of the interface to a value intermediate between the fast and slow wind speeds. When the increased wind pressure in the compression region becomes large enough, it drives a 'forward' shock into the slow wind and a 'reverse' shock into the fast wind. Initially (at small r) both shock normals are approximately in the **n** direction. With the geometry appropriate near solar minimum, the reverse shocks propagate into the fast streams toward high latitudes, either north or south of the streamer belt. The forward shocks propagate toward lower latitudes into the streamer belt. At large r the reverse shocks may propagate substantially above the maximum latitude of the original stream interface. It is noteworthy that Ulysses observed mostly reverse shocks at latitudes above 35° (Gosling *et al.*, 1995). For intermediate values of $|\mathbf{n} \cdot \mathbf{e_r}|$, both fast and slow flows are deflected at the stream interface, in opposite directions, to acquire latitudinal and azimuthal velocity components within the CIR between the forward and reverse shocks. These account for the E/W and N/S flows observed in CIRs. These flows, and the shock strengths, may be interpreted as resulting from conservation of momentum as the fast and slow streams collide. Clearly the interaction is strong if the inclination of the stream interface to the equator on the source surface is large. Then $|\mathbf{n} \cdot \mathbf{e_r}|$ increases to $\sim O(1)$ within ~1–2 AU as the Archimedes spiral wraps into the azimuthal direction. If the inclination is small, the interaction region only develops at larger r due to the spherical expansion of the wind. Any small wiggle in the stream interface at the source surface creates an interaction region if fast wind trails slow wind, although it may be of small spatial extent. The structure and numerical modeling of CIRs is discussed in depth in the article by Gosling and Pizzo (1999).

Depending on the inclination and pattern of the HCS at the source surface, the thickness of the streamer belt, and the location of the spacecraft, a spacecraft may observe the full interaction region, including both shocked and unshocked slow and fast wind, both shocks, and the HCS. At latitudes above that of the original stream interface, it may observe only shocked and unshocked fast wind separated by the reverse shock. Or at even higher latitudes it may observe no plasma signature of the CIR. Of course more than one full or partial interaction region may be observed with each solar rotation. During the first portion of the Ulysses trajectory to high (southern) latitudes, the spacecraft encountered a relatively stable and very impressive CIR, which it observed from early 1992 at ~10° S to late 1994 at ~80° S. The signatures of the CIR, with 26-day periodicity, were observed through nearly 30 solar rotation periods. This sequence of 26-day periods of observation were numbered sequentially and became the focus of the original workshops held at

Elmau Castle. We begin this Chapter with Sect. 2 by Roelof *et al.* presenting three of these periods: CIR 9 at $\sim 24^{\circ}$ S, CIR 18 at $\sim 40^{\circ}$ S, and CIR 25 at $\sim 60^{\circ}$ S.

CIR 9 is characteristic of the periods which show the complete interaction region formed between fast wind from the southern coronal hole and the slow wind from the streamer belt. It includes the shocked and unshocked streams, the forward and reverse shocks bounding the compressed shocked flows, and the HCS. It also shows the ions and electrons accelerated at the shocks; the reverse shock dominates electron acceleration and the acceleration of ions to energies above ~ 1 MeV/amu. Finally, it reveals the modulating influence of the CIR on galactic cosmic rays (GCR), which are suppressed in the CIR and trailing fast wind. CIR 18 is south of the highest southern latitudinal extent of the stream interface; the only clear plasma and field signature is a weak reverse shock. However, accelerated ions and electrons are evident at the shock and extending into the region upstream of the shock, and GCR are modulated in the vicinity of the shock. CIR 25 reveals no clear plasma signature of the CIR. Nevertheless, it does show the clear presence of a broad spatial extent of accelerated ions and electrons, and weakly modulated GCR.

A major theme of the workshops and this chapter is the access of energetic particles accelerated at the shocks bounding the CIR at lower latitudes to high latitudes, well above any plasma signature of the plasma interaction. A related question is the origin of the small but significant 26-day variation of galactic cosmic rays observed at the highest latitudes explored by Ulysses. According to the simplest picture, magnetic fields lie on cones of constant heliographic latitude and do not allow direct magnetic connection to high latitudes from the CIRs at lower latitudes. The reverse shock does extend above the stream interface, but is weak at these latitudes and is not expected to extend very high in latitude. In Sect. 3, four ideas or constraints concerning the latitudinal transport of energetic particles are presented. In Sect. 3.1 Fisk describes the possible direct magnetic connection from Ulysses to a distant portion of the CIR at lower latitudes due to differential rotation of the Sun and non-radial expansion of the fast wind from coronal holes. A constraint on distant magnetic connection to account for the particle enhancements is the energy loss suffered by particles in the solar wind as they propagate from the CIR to Ulysses. In Sect. 3.2 Roelof presents a derivation of that energy loss rate and finds that it favors electrons which are faster. Electrons would then be expected to lag ions, as observed at high latitudes by Ulysses, since they can connect to more distant portions of the reverse shock. Another possibility for latitudinal transport of energetic particles and cosmic rays to high latitudes is diffusion perpendicular to the average magnetic field due to the 'random walk' of field lines. This possibility is explored by Kóta and Jokipii in Sect. 3.3. The origin of stochastic field lines in the solar wind is discussed by Lou in Sect. 3.4.

In Sect. 4 we turn our attention to the observations of Ulysses in the northern hemisphere, the CIR observed in 1996–1997, and a comparison between that CIR and the CIR observed in 1992–1993 in the southern hemisphere. In Sects. 4.1 and

4.2 Sanderson and Forsyth compare the inferred shape of the HCS at the source surface during the north and south CIRs. The northern CIR occurs close to solar minimum when the current sheet is weakly warped. Thus, we expect the CIR that develops in the vicinity of Ulysses to be weak, and indeed the energetic particle enhancements associated with the northern CIR are about two orders of magnitude smaller than those associated with the southern CIR described earlier in the chapter. In contrast, the inferred current sheet at the source surface during the southern CIR is strongly warped, implying a strong CIR in the vicinity of Ulysses. Sanderson and Forsyth show that in all cases the warps in the current sheet determine the dependence of the CIR on helio-longitude, as expected. As the current sheet evolves, so does the longitude of the CIR. In Sect. 4.3 Simnett, Roelof and Heber describe the energetic electron and proton intensity increases during the northern CIR. The enhancements are qualitatively similar to those in the southern CIR (peak intensities associated with the shocks, electrons lag protons at high latitudes) but much smaller.

In Sect. 5 McKibben describes the variation of galactic cosmic rays during the northern CIR. The 26-day variation of the GCR extends to the highest latitudes. An interesting global feature of the GCR observed during the fast latitude scan in early 1995 is their dependence on heliographic latitude. Their intensity increases symmetrically with increasing latitude but with a minimum intensity at a latitude of $\sim 10^{\circ}$S, so that the intensity maximum in the northern polar regions is larger than that in the southern polar regions. There is currently no explanation for this offset.

2. Global Structure, Observations and Challenges to Theory

E. C. ROELOF, G. M. SIMNETT, T. R. SANDERSON, and H. KUNOW

2.1. INTRODUCTION

The Ulysses mission made its first southern pass during the declining phase of Solar Cycle 22. It is in the decline of each solar cycle that transient activity diminishes while the streamer belt shrinks towards the equator. This extends the boundaries of the polar coronal holes (PCH) towards the equator. In fact, towards the end of the decline to solar minimum, each PCH can actually cross the equator, forcing the streamer belt to ripple into an equator-crossing sinusoid in latitude. The interaction of the high-speed solar wind from the PCHs with the low-speed solar wind from the streamer belt forms the recurrent CIR structure. After its Jupiter flyby flung Ulysses out of the ecliptic in February 1992, it performed a surgical cut in latitude through the three-dimensional configuration of the CIRs that were well established in Solar Cycle 22. Ulysses made the transit to mid-latitudes at helioradii that varied only from 5.3 AU on CIR 1 (June 1992) to 4.3 AU on CIR 18 (September 1993). We have a century of observations which demonstrate that the

CIR structure is remarkably stable; this was established once the cause of 27-day recurrent geomagnetic disturbances were demonstrated to be CIRs. Consequently, Ulysses gave us an almost purely latitudinal slice at $\sim$5 AU of the approximately time-stationary structure of the heliosphere during the declining phase of the solar cycle. Even more fortunately, Ulysses carried a well-conceived complement of particles and fields instruments that could characterize its environment in terms of the magnetic field, the solar wind plasma, and energetic particles from galactic cosmic ray protons with energies $>$1 GeV down to CIR-associated $\sim$50 keV electrons and ions.

In the following section these comprehensive measurements are presented and interpreted.

2.2. OBSERVATIONS

As a result of the cooperation of the two workshops on CIRs convened at Elmau, Germany, in 1996 and 1997, a standard one-page data format was developed to represent each CIR from CIR 1 (June 1992) through CIR 36 (December 1994). The data were measured by the Ulysses spacecraft on its first (southern) excursion into the high-latitude heliosphere. These plots were constructed by C. Tranquille of ESA/ESTEC and archived in the Ulysses Data System. The 26-day time-ordered format displays the history of mostly one-hour averages for a wide range of energetic particle, plasma and magnetic field parameters measured by Ulysses, which characterize the dynamics of each CIR. Details of the Ulysses intrumentation may be found in the special volume of *Astron. and Astrophys.* **92**, 207–440, 1992.

Examples of the one-page 26-day summaries are presented in Figs. 1, 2, and 3 for representative CIRs 9, 18, and 25, respectively. The abscissa is triply labeled by day of year (with the date of the start of each rotation indicated on the left), heliocentric distance (in AU) of Ulysses, and Ulysses latitude (in degrees). The time resolution of the data is one hour (with one obvious exception). The top panel shows unidirectional differential intensities of ions (HI-SCALE), beginning at 61–77 keV, jumping to 207–336 keV, and then extending to protons at 0.48–0.97 MeV. The series is continued with protons (COSPIN/LET) 1.2–2.0 MeV and 8–19 MeV. These energies cover a proton velocity range of a factor of 20 ($0.01 < \beta < 0.20$). The second panel depicts the percentage modulation of 0.25–2 GeV ($0.60 < \beta < 0.94$) galactic cosmic ray protons (COSPIN/KET) in daily averages de-trended from the effects of the monotonic latitudinal gradient. The third panel is devoted to four electron channels (HI-SCALE) covering the range 30–300 keV, corresponding to $0.34 < \beta < 0.80$. All the energetic particle channels contain instrumental backgrounds that have not been completely subtracted (as indicated where the traces are horizontal). Thus the top three panels depict the behavior of CIR-associated energetic particles whose velocities vary by a factor of nearly 100.

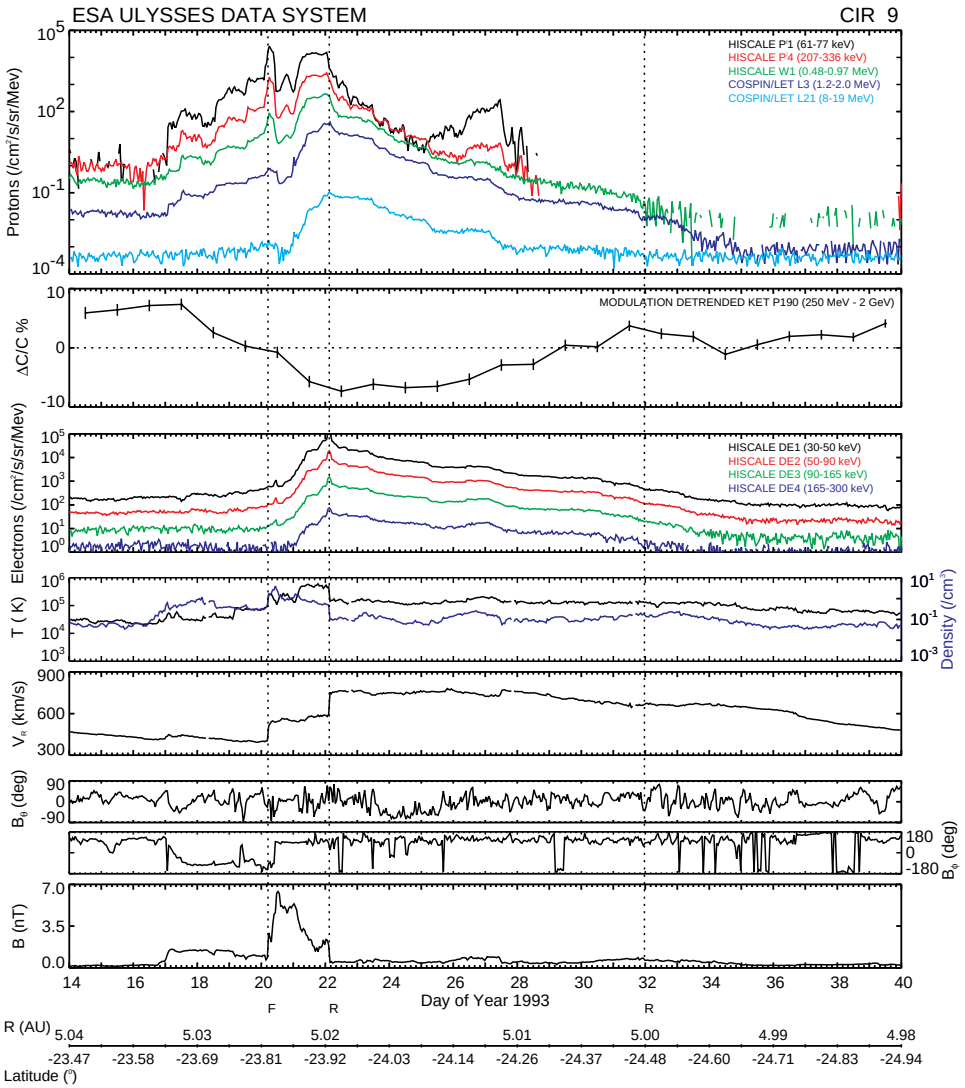

Figure 1. CIR 9 as observed by Ulysses in January 1993 at a distance of ∼5 AU and 24° heliolatitude. Forward and reverse shocks during the 26 day period from January 14–February 09 are marked. *Panel No. from top:* (1) Proton fluxes of various energy channels observed by HI-SCALE and COSPIN. (2) Modulation dependent high energy proton channel (250 MeV–2 GeV) showing CIR related modulation (daily averages). (3) CIR related electron increases in various energy ranges observed by the HI-SCALE experiment. (4) Solar wind temperature and density. (5) Solar wind speed. (6) Magnetic field elevation. (7) Magnetic field azimuth. (8) Magnitude of magnetic field (HED experiment). All data points are hourly averages except for daily averages in Panel No. 2.

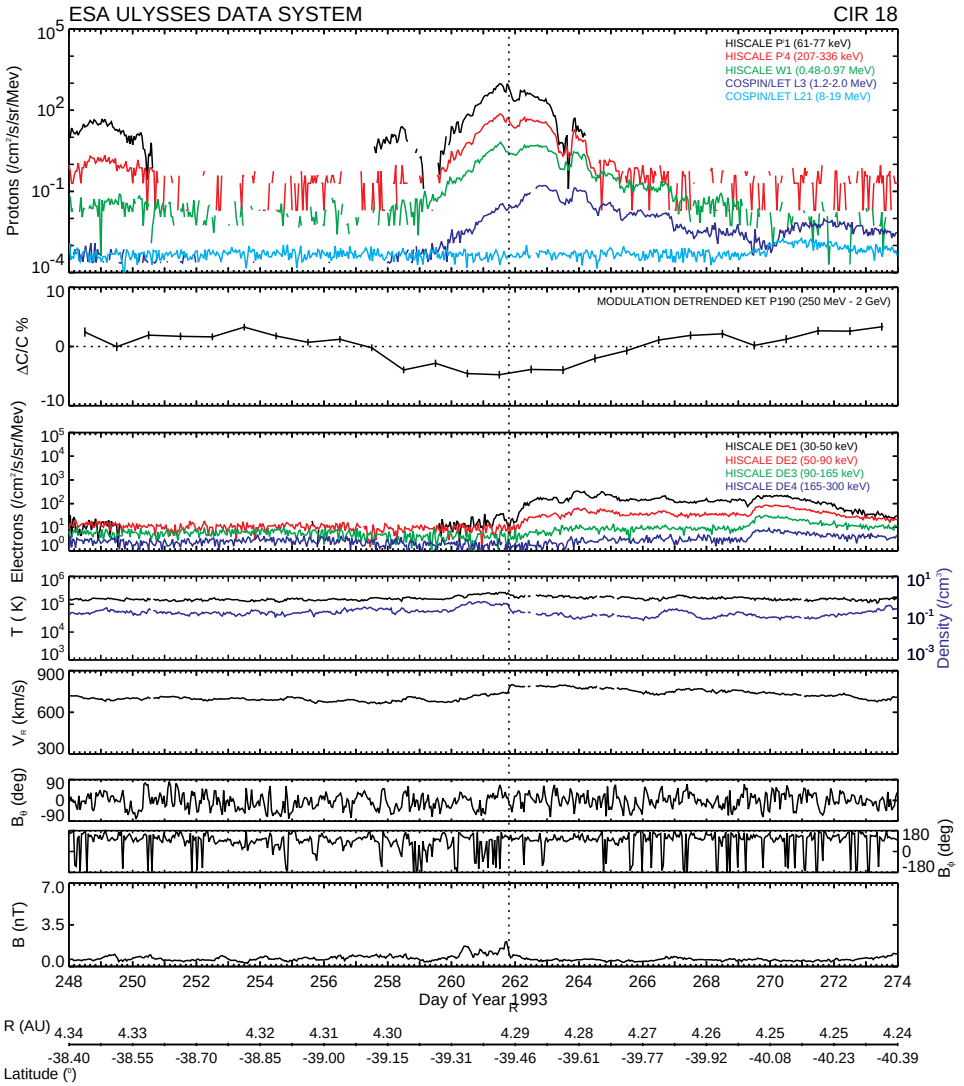

Figure 2. CIR 18 as observed by Ulysses in September 1993 at a distance of 4.3 AU and 40° south heliolatitude. Averages of observations are plotted from September 5–October 1, 1993. For details see caption of Fig. 1.

The plasma (SWOOPS) and magnetic field parameters (HED) form the lowest 5 panels: solar wind density (cm^{-3}) and temperature (K), and radial velocity (km/s); and magnetic field magnitude (nT) and directions (θ and ϕ in degrees) in RTN coordinates (θ is latitude measured from the R–T plane and ϕ is longitude in the R–T plane measured from the negative T direction). Vertical dashed lines indicate shocks identified by Balogh *et al.* (1995a) up until day 335 of 1993; thereafter they represent reverse waves (that have not formed shocks).

CIR 9, shown in Fig. 1, is representative of the strong CIRs seen as Ulysses was about to leave the streamer belt and rise above the heliospheric current sheet. Note that positive polarity (away from the Sun) was only observed for one 3-day stretch (days 17–20), while the remainder of the polarity was negative (towards the Sun). The southern polar coronal hole exhibited negative magnetic polarity during the decline of Solar Cycle 22. The solar wind exhibits the wide range of velocities experienced in this transition region: $\sim$400 km/s in the streamer belt to $\sim$800 km/s in the polar hole stream. This factor-of-two variation produces the strong forward and reverse shocks on days 20 and 22, respectively, that bound the magnetic compression region of the CIR (also clearly identifiable in the enhanced density and temperature).

Burton *et al.* (1996) have identified these boundary-layer shocks as super-critical. Low-energy ions have comparable peaks downstream of both forward and reverse shocks, but $>$1 MeV protons, $>$30 keV electrons, and the modulation of $\sim$1 GeV galactic cosmic ray protons respond much more strongly downstream of (preceding) the reverse shock. All particle species are affected a few days upstream of (before) the forward shock, but the particle effects extend a good 10 days upstream of (after) the reverse shock. Note that all the ions and electrons in the top two panels decay at roughly the same rate. In this decay phase, the distance from Ulysses to the reverse shock along the interplanetary field lines is steadily increasing as the shock corotates away from Ulysses.

Contrast CIR 9 at 24°S with CIR 18 at 39°S, as shown in Fig. 2. Now Ulysses is wholly in the southern polar high speed stream. The only signature of the CIR in the plasma data is a small reverse shock late on day 261 (only 3 more reverse shocks were identified after CIR 18). Yet the CIR signature is still clear in the energetic particles and galactic cosmic ray protons. However, the $<$100 keV ions now decay much more rapidly than the 8–19 MeV protons (which peak a day after the reverse shock). The 30–300 keV electrons reach their maxima many days after the reverse shock, and then their intensities decay very slowly. This lag of the $\sim$50 keV electron intensity maxima several days behind that of the $\sim$1 MeV protons appears abruptly after CIR 13 and persists to the highest latitudes at which the protons are measurable above instrument background (CIR 28 at 67°S).

These patterns become even more exaggerated when we examine CIR 25 at 56°S in Fig. 3. Now there is only a weak reverse wave (day 69) formed by a $\sim$100 km/s variation in the solar wind velocity. Nonetheless, all particle species show strong variations, although the maxima (or GCR minimum) are many days after the wave. The low-energy ions decay rapidly, while the 1.2–2 MeV protons and the 30–300 keV electrons have a remarkably symmetrical time (longitude) dependence that extends over most of the rotation (270°). Simnett *et al.* (1995b) showed that the H/He ratio (not shown) measured at 0.35–1.0 MeV/amu decreased steadily following the reverse wave, reaching values $<$10 at about the time of the electron intensity maximum.

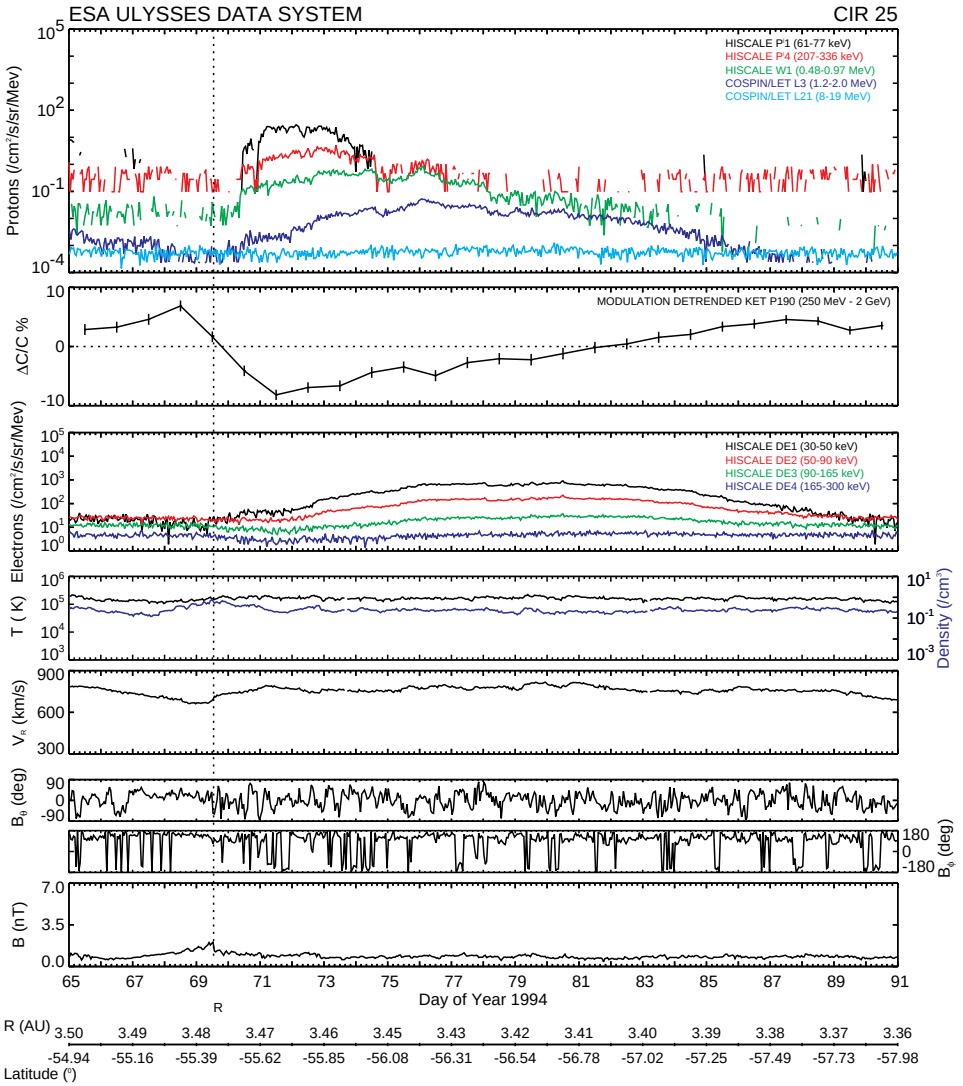

Figure 3. CIR 25 as observed by Ulysses in March 1994 at a distance of 3.5 AU and 56° south heliolatitude. Averages of observations are plotted from March 4–March 31, 1994. For details see caption of Fig. 1.

Note that the phase of the particle maxima (or GCR minimum) for each species has remained almost the same in rotations 9, 18, and 25, even though Ulysses has climbed from 24° S up to 56° S and decreased its helioradius from 5.0 to 3.5 AU over 3/4 of a year. Although the shapes of the intensity histories of each species have evolved over the solar rotations, examination of the traces in the top two panels of Figs. 1, 2, and 3 shows a systematic 'morphing' of the shape of the uppermost trace (61–77 keV ions with $\beta = 0.01$) into that of the lowermost (165–300 keV electrons with $\beta = 0.80$). Thus, on any given rotation from CIR 9 to CIR 25, the energetic

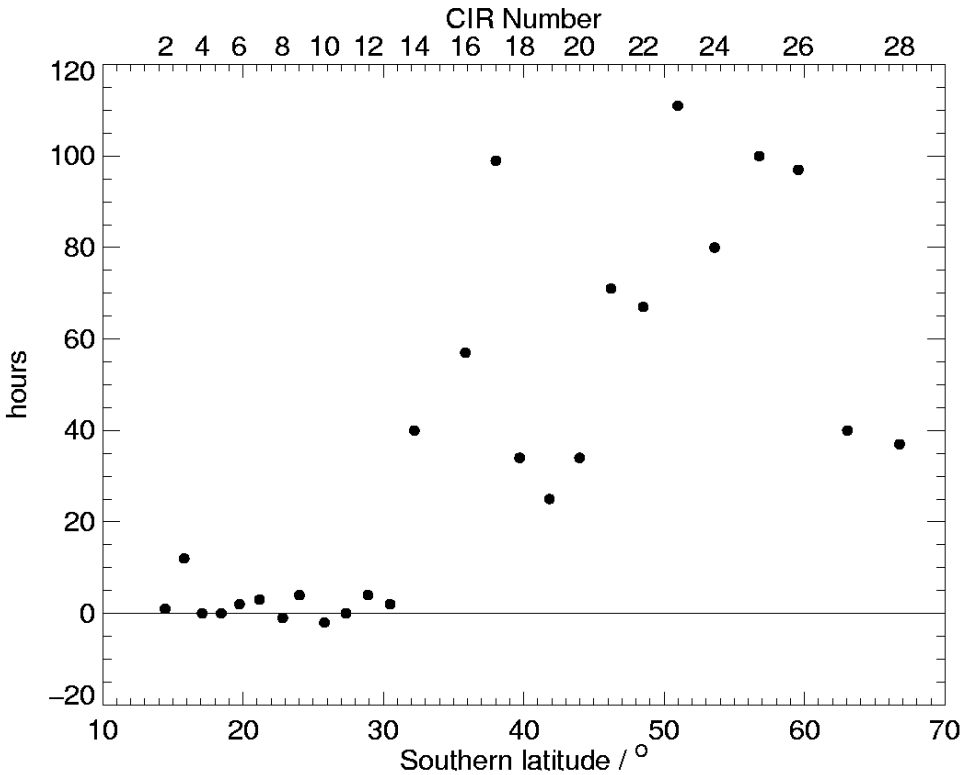

Figure 4. Difference in time between 12 hour mean maxima of ∼1 MeV/amu ions and electrons (positive times correspond to ions arriving first). No value plotted for CIR 15 as it was distorted by a transient solar energetic particle event. The value for CIR 23 was determined by measuring the shift between the centroid at half the maximum values (from Sayle and Simnett, 1998).

particle behavior is systematically ordered by the particle velocity. We shall see in Sect. 3 below that the dominant trends in these energetic particle time histories can be explained as the consequence of remote magnetic connection of Ulysses at high latitudes to the CIRs that exist at lower latitudes, combined with the inescapable process of particle energy loss due to organized magnetic gradient and curvature drifts in the solar wind electric field (see Sects. 3.2 and 3.3).

One remarkable trend in the energetic particle data that has very strong implications for the nature of the global magnetic field configuration is displayed in Fig. 4 from Sayle and Simnett (1998). We mentioned in our description of CIR 18 the abrupt appearance after CIR 13 of the lags of the ∼50 keV electron intensity maxima behind those of the ∼1 MeV protons. It is evident from Fig. 4 that lags as great as 4 days were already observed by CIR 17 (37° S), whereas from CIR 2 up to CIR 13 (30° S), no lags were observed. Therefore, this abrupt effect, indicative of remote magnetic connection from Ulysses to the CIRs, appears suddenly within a latitude interval of only 7°.

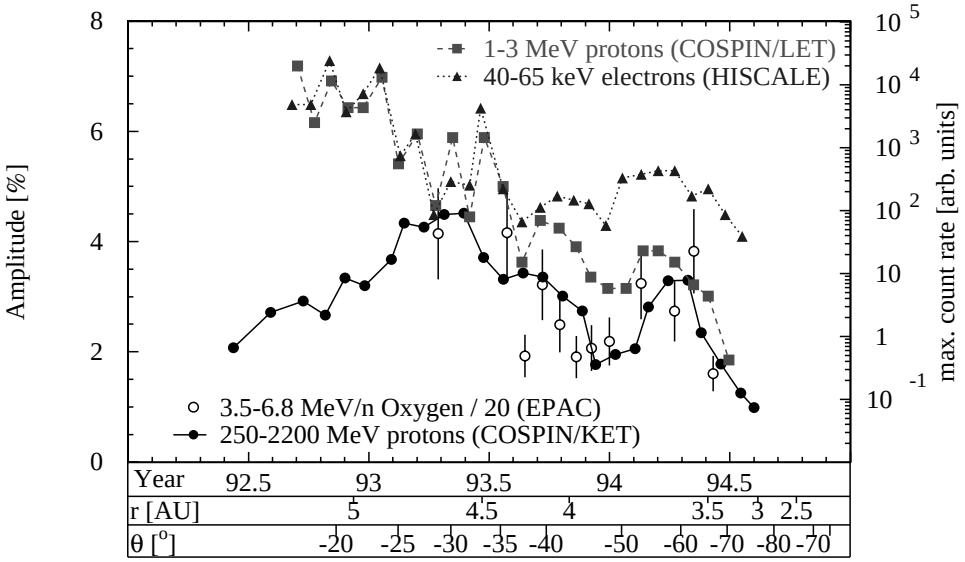

Figure 5. Maximum amplitudes of CIR accelerated protons and electrons and CIR modulated galactic protons from mid-1992 through mid-1994 (from Heber *et al.*, 1999).

Another striking correlation between diverse particle species is displayed in Fig. 5 from Heber *et al.* (1999). It compares the normalized intensity maxima of 1–3 MeV protons (COSPIN/LET), 3.5–6.8 MeV oxygen (EPAC) and 40–65 keV electrons (HI-SCALE) with the maximum amplitude of the 0.25–2.2 GeV galactic cosmic ray protons (COSPIN/KET). Maxima are plotted for CIRs 1 through 27 (13° S to 63° S). The energetic particle intensities are not correlated with the GCR amplitude until Ulysses begins to depart the streamer belt and to enter the southern polar high-speed stream around CIR 13 (30° S). From then on, right up to the highest latitudes where the energetic particles can be measured, their intensity maxima track those of the GCR 26-day amplitude. This correlation exists among particles whose magnetic rigidities (the usual parameter of galactic cosmic ray modulation theory) vary over a range of 0.18 to 880 MV/c (which is a factor of almost 5000).

A final observational correlation can be seen in Fig. 1. Comparing the history of the 61–77 keV ion intensities (top panel) between the forward and reverse shocks (day 20–22) with that of the solar wind plasma temperature (fourth panel down) shows they are quite similar. Incidentally, with respect to the relationship between energetic particle intensities discussed by D. S. Intriligator in Crooker, Gosling *et al.* (1999), there are three stream interfaces in CIR 9 (Wimmer-Schweingruber *et al.*, 1997): two fall in the two intensity (temperature) local minima, and the third is later. The top panel of Fig. 1 reveals that the highest energy protons are unaffected by the second and third stream interfaces. Ogilvie and Roelof (1999) have made detailed temperature/intensity comparisons for CIRs 5–13, and they find in the strongest CIRs (*e.g.* those with supercritical reverse shocks) that a good

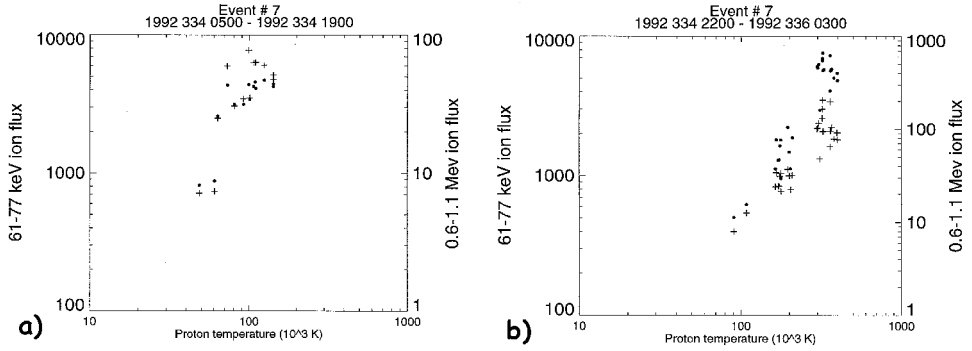

Figure 6. Ion fluxes *vs.* proton temperatures for CIR 7 following the forward shock (a) and preceding the reverse shock (b).

correlation exists between the logarithm of the 61–77 keV ion intensity and the logarithm of the plasma temperature. An example is shown in Fig. 6 for CIR 7. More complete particle and plasma data for this CIR are given in a figure of the article by Crooker, Gosling *et al.* (1999). On the scatter plot of Fig. 6, hourly averages of the temperature are plotted against the 61–77 keV ion intensity (plotted as dots). The intensities of 0.6–1.1 MeV protons are also plotted *vs.* temperature (as plusses). Two time periods are plotted; first, between the forward shock and the stream interface; and second, between the stream interface and the reverse shock. Note that the particle intensities vary by a factor of $\sim$30. The general result of Ogilvie and Roelof (1999) is that the temperature correlation is best at the lower energies and prior to the reverse shock. Without going into their explanation in terms of the shock acceleration mechanism, one can draw a model-independent conclusion. The ions that are first seen following the stream interface must have traveled from the reverse shock to Ulysses along magnetic lines with velocities about ten times greater than the plasma velocity. On the other hand, the temperature is a parameter that is transported with the solar wind, and it must carry with it the signature of the shock heating (decreased in a calculable way by adiabatic cooling en route). However, the plasma also carries the magnetic field line with it. In a corotating frame, both the plasma and the energetic particles follow the field line; the particles just move along it faster than the plasma. Therefore, if there is a correlation between plasma temperature and energetic particle intensity, there cannot be any significant transverse transport of the energetic ions within the CIR between the reverse shock and the spacecraft.

2.3. Observational Challenges to Theory

The following salient observational points characterize the phenomenology of CIRs as manifested in measurements of the magnetic field, solar wind plasma, galactic cosmic ray protons, and low-energy ions and electrons. Not only do the striking inter-relationships among these diverse measurements demand explanation, their

latitude dependence has profound implications for the three-dimensional structure of the heliosphere during the declining phase of the solar cycle.

- Continuation to highest latitudes of: 26-day recurrent modulation of ∼1 GeV galactic cosmic ray protons and ∼50 keV electron events (in relative phase with each other). Phase of ∼50 keV electron maximum consistent with a cylindrical (latitude-independent) corotating structure (Roelof *et al.*, 1996).
- Lag of ∼50 keV electron maxima 1–4 days behind ∼1 MeV proton maxima suddenly appears at mid-latitudes ∼32° S on CIR 14 (Sayle and Simnett, 1998).
- Sudden change in 26-day GCR modulation amplitude, also above ∼30° S (Heber *et al.*, 1999).
- Diminution of ∼1 MeV proton and ∼50 keV electron intensities by a factor $\sim 10^{-4}$ with increasing southern latitude 25° S–80° S.
- H/He ratio at ∼1 MeV/amu is <10 near the reverse shock (*vs.* 20 for solar energetic particles) (Simnett *et al.*, 1995b).
- Nearly symmetrical longitude (time) profiles extending over almost 360° in 26-day recurrent modulation of ∼1 GeV GCR protons and ∼50 keV electron events.
- Amplitude of 26-day GCR modulation correlated with GCR latitude gradient (Kunow *et al.*, 1997; Zhang, 1997).
- Amplitude of 26-day GCR modulation correlated with maximum intensities of ∼50 keV electrons and ∼1 MeV protons (Heber *et al.*, 1999).
- Highest intensities of ∼50 keV electrons and ∼1 MeV protons associated with the reverse shock (when shocks can be observed < 45° S), rather than the forward shock.
- Energetic ion intensities (50 keV–5 MeV) exhibit minima between forward and reverse shock (sometimes in vicinity of stream interface).
- At strongest CIRs (20° S–30° S), solar wind plasma temperature is correlated logarithmically with the intensity of 60 keV ions and 1 MeV protons downstream of shocks (best correlation between stream interface and reverse shock).

2.4. DISCUSSION

Let us see how the theoretical explanations of the following sections (and those of other chapters as well) fare in addressing the patterns summarized immediately above in Sect. 2.3.

1. High-latitude particle events and GCR modulation imply remote magnetic connection. This requires drastic modification of the Parker Archimedean spiral field. Fisk (Sect. 3.1) and Kóta/Jokipii (Sect. 3.3) offer distinctly different models that are deterministic *vs.* stochastic (respectively).
2. No explanation is offered for the sudden appearance of electron lag at ∼32° S.
3. No explanation is offered for the sudden change of the GCR modulation amplitude at ∼32° S.

4. Diminution of particle intensities with increasing latitude is consistent with an energy-loss mechanism that depends only on velocity (but is mass- and charge-independent). This agrees with the theory of Roelof (Sect. 3.2) and calculations of Kóta/Jokipii (Sect. 3.3).
5. H/He ratios <10 are consistent with a large contribution of accelerated pickup ions (Gloeckler, 1996).
6. Symmetrical high latitude electron and ion profiles are implied by the Fisk model connection (Fig. 7), but this has not been combined with energy loss calculation to demonstrate quantitative agreement with data.
7. Zhang/Simpson offer a theory for the GCR amplitude/gradient relationship (McKibben, Jokipii *et al.*, 1999).
8. No explanation offered for the correlation between GCR modulation and low-energy ion increases. Correlations have been observed for decades in the ecliptic between Forbush decreases and energetic storm particle ion events (although electron increases were rarely observed).
9. Giacalone and Jokipii (1997) offered a simple explanation for the reverse shock being more efficient than the forward shock (seed particles have higher upstream energies because of the higher solar wind velocity at the reverse shock). However, no shock acceleration theory published so far explains all the details of shock-associated ion spectra (Desai *et al.*, 1999; Fisk and Lee, 1980).
10. The conjecture by Siscoe and Intriligator (1993) (put forward and subsequently rejected in their original study) was that the stream interface, comprising unshocked plasma, should be a 'gap' in energetic ions accelerated at the forward shock and the reverse shock. (This is discussed in Crooker, Gosling *et al.*, 1999, by Intriligator.) However, many CIRs do show gaps, as predicted.
11. The correlation of plasma temperature with energetic ion intensities on an hour-by-hour basis (Ogilvie and Roelof, 1999) is consistent with the original 'gap' conjecture of the low-energy particle intensity minimum in the vicinity of stream interface(s). However, this correlation is clearest only for the strongest (mid-latitude) super-critical shocks.

3. Remote Connection of Particles at High Latitudes to CIRs

J. KÓTA, L. A. FISK, J. R. JOKIPII, Y.-Q. LOU and E. C. ROELOF

There have been several ideas proposed to explain the particle transport from the CIRs at low latitudes to Ulysses at high latitude. The possible mechanisms outlined below are not mutually exclusive; a combination of these may occur. Further studies are needed to explore the quantitative contribution from these phenomena.

3.1. LATITUDE TRANSPORT BY DIRECT MAGNETIC CONNECTION

L. A. FISK

The ability of low-energy particles to propagate from CIRs near the equatorial plane to high heliographic latitudes would obviously be greatly facilitated if there was a direct magnetic connection from low to high latitudes. In a standard Parker model for the heliospheric magnetic field, such direct connection is prohibited since the field lines lie on cones of constant latitude. However, as was pointed out by Fisk (1996), the interplay between the differential rotation of the photosphere and the non-radial expansion of the solar wind from more rigidly rotating polar coronal holes can lead to large excursions of the heliospheric magnetic field in latitude. In an introductory paper to this volume, Fisk and Jokipii review the model of Fisk (1996), describe its basic assumptions, and provide some illustrative field configurations. The basic consequence of the model is that the heliospheric magnetic field acquires a systematic component in the polar direction, which results in direct magnetic connection from low to high latitudes.

In this section, we explore the consequences of the model of Fisk (1996) for the observed properties of energetic particle events seen at high latitudes. The properties, with which the model should be consistent, include: the attenuation of the particle intensity with latitude, the observed behavior with longitude, including the asymmetry in the intensity in longitude, and phase differences between electrons and protons.

Shown in Fig. 7, from Zurbuchen *et al.* (1999) and repeated from Fisk and Jokipii (1999), are the heliocentric radial distances at which a field line from a given latitude and longitude on the Sun (following the non-radial expansion) will cross a heliocentric latitude of 30°, *i.e.* will enter into the region where CIRs occur. This calculation assumes a simple model for the excursions of the magnetic field lines at the Sun, in which these excursions are circles offset from the rotation axis, as is described in Zurbuchen *et al.* (1997). The actual distance along the field line is, of course, much longer than the heliocentric radial distance, since the field follows the general spiral pattern. Within the first 15 AU in radial distance from the Sun, the distance along the field is approximately twice the radial distance; at larger radial distances, the distance along the field is a larger multiple.

Ulysses would observe the various longitudes in Fig. 7 by traversing from right to left; the longitudes are defined relative to the rotating Sun and are of arbitrary phase. Thus, when Ulysses passes through the longitude region around 200°, field lines at all latitudes are at their point of closest approach in connection distance to the CIR.

We should expect then in this model, as is observed, that the longitudinal phase of energetic particle events generated by acceleration at the CIRs, or for that matter galactic cosmic ray modulation resulting from the CIR, is essentially independent of latitude. Moreover, the intensity variation with latitude should be approximately correct. The mean free path of low-energy particles in the heliosphere is $\sim$1 AU.

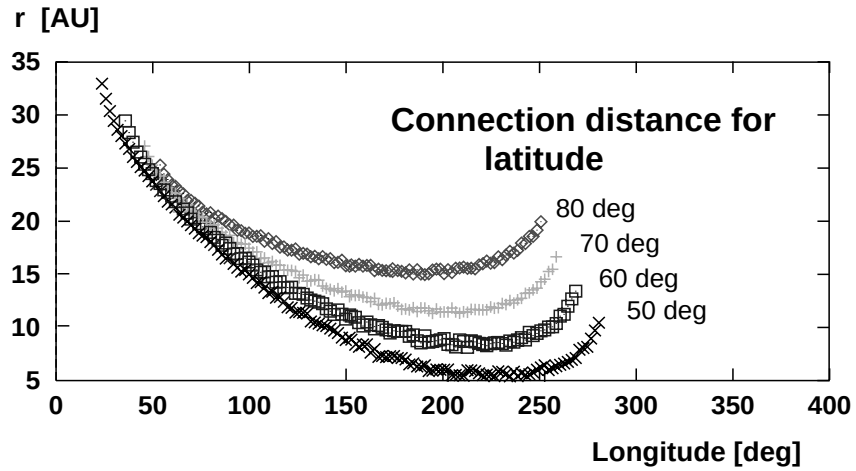

Figure 7. The heliocentric radial distance at which a field line from a given latitude and longitude crosses 30° north latitude, *i.e.* enters the region where CIRs occur. The longitude scale is fixed on the rotating Sun, and is of arbitrary phase (after Zurbuchen *et al.*, 1999, see also Fig. 5 of Fisk and Jokipii, 1999, in this volume).

Thus, for low-latitude field lines, which connect within 5–10 AU in radial distance, or 10–20 AU along the field lines, there is attenuation due to scattering and adiabatic deceleration, but it is not extensive. For higher latitude field lines, the distance along the field line to the CIR increases to ∼30 AU, and the attenuation due to scattering and adiabatic deceleration is considerably greater. Indeed, high latitude events can be four orders of magnitude smaller than their low-latitude counterparts (Roelof *et al.*, 1997).

There is also an interesting asymmetry in Fig. 7. As Ulysses traverses from right to left, the onset of field lines that have a reasonable connection distance to the CIR region is quite abrupt. However, as Ulysses continues to traverse in longitude, the increase in connection distances, to where it is no longer reasonable to expect that energetic particles from the CIR can be observed, is fairly gradual. We should thus expect that the onset of the observed energetic particle events would be more abrupt than their decay, and indeed that is observed (Simnett *et al.*, 1995a). Such asymmetry may be difficult to account for in models in which the latitude transport is due primarily to cross-field diffusion, since in such a process a more symmetric profile might be expected.

The actual profiles that should be observed for electrons and protons will depend on a number of competing effects. The intensity of accelerated particles at the shocks surrounding CIRs should, at least initially, increase with heliocentric radial distance as the CIR develops. Thus, as field lines connect to the CIR further out in radius, the intensity should tend to increase. Scattering along the field lines and adiabatic deceleration will have the opposite effect of decreasing the intensity. This reduction should be stronger for protons than for the more mobile electrons. Thus, as Ulysses moves across Fig. 7 from field lines that have short connection distances

to the CIR to field lines with longer connection distances, it should see the proton peak first, followed by the electron peak, as is observed (Simnett *et al.*, 1995a).

Conceptually, then, there are a number of aspects of the model for the heliospheric magnetic field with footpoint motion that are consistent with the observations of energetic particles in CIRs. However, it should be noted that, in this discussion of the behavior of the energetic particle events with longitude, the model used is quite simple. We consider that a field line which connects below 30° in latitude will encounter the CIR and be able to acquire energetic particles accelerated at the CIR. In fact, CIRs have considerable variation in longitude and radial distance. There is a difference between the ability of the forward and reverse shocks to accelerate particles, with the latter generally a better accelerator. There is considerable structure both in longitude and latitude as high- and slower-speed solar wind interact. A detailed modeling of the field configuration in a realistic three-dimensional solar wind, and its consequences for energetic particle propagation to high latitudes, is required.

3.2. Adiabatic Energy Losses of Charged Particles

E. C. ROELOF

Clearly the rate of energy loss of particles propagating from a distant point on the CIR to the inner heliosphere will determine in part their observed intensity at a given energy. Northrop (1963) summarized the equations governing the motion of a charged particle in the adiabatic (guiding center) approximation for the case when the transverse electric field is 'small', *i.e.*, when the electric field drift velocity $\mathbf{u}_E = \left(c/B^2\right)\mathbf{E}\times\mathbf{B}$ is much smaller than the particle velocity $\mathbf{v} = v_{\|}\mathbf{b} + \mathbf{v}_{\perp} + \mathrm{d}\mathbf{R}_{\perp}/\mathrm{d}t$. Here $\mathbf{v}_{\perp}$ describes the gyration of the particle about the guiding center motion $\mathbf{R}$(t). The time rate of change along a particle's trajectory of its kinetic energy $T = (m - m_{\circ})\,c^2 = (\gamma - 1)\,m_{\circ}^2$ is given by

$$\frac{\mathrm{d}T}{\mathrm{d}t} = q\mathbf{E}\cdot\frac{\mathrm{d}\mathbf{R}}{\mathrm{d}t} + \frac{mv_{\perp}^2}{2}\frac{\partial \ln B}{\partial t} \tag{1}$$

$$\frac{\mathrm{d}\mathbf{R}}{\mathrm{d}t} = v_{\|}\mathbf{b} + \mathbf{u}_E + \left(\frac{mc}{qB}\right)\mathbf{b}\times\left(\frac{v_{\perp}^2}{2}\nabla \ln B + v_{\|}\frac{\mathrm{d}\mathbf{b}}{\mathrm{d}t} + \frac{\mathrm{d}\mathbf{u}_E}{\mathrm{d}t}\right) \tag{2}$$

where $\mathbf{b} = \mathbf{B}/B$ is the magnetic field unit vector, and the total derivative $\mathrm{d}/\mathrm{d}t = \partial/\partial t + (v_{\|}\mathbf{b} + \mathbf{u}_E)\cdot\nabla$ is taken along the guiding center trajectory (neglecting additional drift terms that are much smaller than the electric field drift). The dominant term in $\mathrm{d}/\mathrm{d}t$ is $v_{\|}\mathbf{b}\cdot\nabla$, except during the short time intervals when the particle is mirroring and $v_{\|} \to 0$. After some vector algebra we obtain

$$\frac{\mathrm{d}T}{\mathrm{d}t} = qv_{\|}E_{\|} + \frac{mv_{\perp}^2}{2}\frac{\partial \ln B}{\partial t} + \mathbf{u}_E\cdot\left(\frac{mv_{\perp}^2}{2}\nabla \ln B + mv_{\|}^2\mathbf{b}\cdot\nabla\mathbf{b}\right) + \ldots \tag{3}$$

where smaller terms have been neglected. The terms inside the brackets become the familiar 'gradient B' and 'curvature' drift velocities if they are divided by qB/c. Now let us divide (3) by T and note that $mv^2/T = \gamma\beta^2/(\gamma-1) = (\gamma+1)/\gamma$. Introducing the pitch cosine μ, we then obtain

$$\frac{\gamma}{\gamma+1}\frac{\mathrm{d}\ln T}{\mathrm{d}t} = \frac{1-\mu^2}{2}\frac{\partial \ln B}{\partial t} + \mathbf{u}_E \cdot \left(\frac{(1-\mu^2)}{2}\nabla \ln B + \mu^2 \mathbf{b}\cdot\nabla\mathbf{b}\right) \tag{4}$$

where we have omitted the $E_{\|}$ term because parallel electric fields are usually small once the solar wind escapes the corona.

The remarkable property of Eq. 4 is that the *RHS does not depend on any* properties of the particle – not charge, not mass, not even velocity. The only velocity-dependent term is $\gamma/(\gamma+1)$ on the LHS, and this varies extremely weakly with velocity, beginning at 1/2 for non-relativistic particles and approaching 1 for extremely relativistic particles. Equation 4 states that the instantaneous *fractional* time rate of change of energy for *any* particle undergoing guiding-center motion depends only on the *local* properties of the solar wind and magnetic field. The reason, then, that 50 keV electrons ($\beta = 0.4$) lose far less energy than 50 keV/amu ions ($\beta = 0.01$) while traveling from a distant CIR connection to Ulysses at 5 AU is that the 50 keV/amu ions take longer to make the transit. Because the fractional loss rate of energy is the same for both the electrons and the ions, the particle that spends the least time in a given region loses the least energy. We can demonstrate this quantitatively with the following computation.

Beyond 5 AU, $\mathbf{u}_E$ becomes just the solar wind velocity $\mathbf{V} = \mathbf{V}(\mathbf{r}/r)$ and reasonable approximations for a low-latitude spiral magnetic field give $\nabla \ln B \cong \mathbf{b}\cdot\nabla\mathbf{b} \cong -\mathbf{r}/r^2$. For the following discussion we will neglect the explicit time dependence of the magnetic field ($\partial B/\partial t \cong 0$), so that substitution in the non-relativistic limit ($\gamma = 1$) of Eq. 4 yields

$$\frac{\mathrm{d}\ln T}{dt} \cong -\frac{V}{r}\left(1+\mu^2\right) \to -\frac{4V}{3r} \tag{5}$$

when one averages μ^2 over an isotropic pitch-angle distribution. This is the usual expression given for what is called 'adiabatic deceleration' in the diffusion convection formulation of cosmic ray transport. Note, however, that we have obtained this result from guiding center motion for the particle, without introducing pitch-angle scattering. Weak scattering would tend to isotropize the pitch-angle distribution, leading to $\langle\mu^2\rangle = 1/3$. However, for any value of $\mu^2 < 1$, $-2V/r < \mathrm{d}\ln T/\mathrm{d}t < -V/r$, so the actual pitch angle distribution makes no more difference than a factor between $3/4$ and $3/2$ times the adiabatic rate.

Let us now examine the effect on a non-relativistic particle traveling from some initial position $\mathbf{r}_1$ to another one $\mathbf{r}_2$ along guiding center trajectory $\mathbf{r}(t)$. If the particle does not mirror along the trajectory, then the fractional energy loss can be expressed as a single-valued function of distance through the relation $\mathrm{d}r/\mathrm{d}t =$

$(\mu v\mathbf{b}+\mathbf{u}_E)\cdot\mathbf{r}/r$. For a local Parker spiral beyond ~3 AU, $\mathrm{d}r/\mathrm{d}t \cong \mu vV/\Omega r\sin\Theta + V$, so that

$$\frac{\mathrm{d}\ln T}{\mathrm{d}r} = \frac{\mathrm{d}t}{\mathrm{d}r}\frac{\mathrm{d}\ln T}{\mathrm{d}t} = \frac{r}{V}\frac{\mathrm{d}\ln T}{\mathrm{d}t}\Bigg/\left(r+\frac{\mu\beta c}{\Omega\sin\Theta}\right) \tag{6}$$

Examination of Eq. 4 shows that for any but the highest latitudes the dominant dependence of $\mathrm{d}(\ln T)/\mathrm{d}t \propto (-V/r)$, so the numerator in Eq. 6 should be a weak function F of $\mathbf{r}$ and μ where $(-F)$ is of order unity. In the denominator, the numerical factor $c/\Omega = 26$ days $\times\, c/2\pi = 714$ AU determines the character of the dependence on β. Non-relativistically $T \propto \beta^2$, so we can rewrite Eq. 6 as

$$\frac{1}{\beta}\frac{\mathrm{d}\beta}{\mathrm{d}r} = -\frac{F(\mathbf{r},\mu)}{r+\mu\beta\,(714\,\mathrm{AU}/\sin\Theta)} \tag{7}$$

where we have taken $\mathbf{b}$ to have positive (outward) polarity, so $\mu > 0$ indicates a particle propagating outward. In order to integrate Eq. 7 for $\beta(\mathbf{r})$ we need to specify how μ depends on $\mathbf{r}$ as well as the equation of the field line $\Theta(r)$. One choice could be scatterfree propagation with $1-\mu^2 \propto B(r)$. Just for the purpose of rough estimation, however, let us treat F and μ as constants. Then the extreme (non-relativistic) limits are:

$$\beta_2-\beta_1 \sim \frac{(-F/\mu)(r_2-r_1)}{714\,\mathrm{AU}} \qquad |\mu|\,\beta \gg \frac{r}{714\,\mathrm{AU}} \tag{8}$$

$$\frac{\beta_2}{\beta_1} \sim \left(\frac{r_2}{r_1}\right)^{-F} \qquad |\mu|\,\beta \ll \frac{r}{714\,\mathrm{AU}} \tag{9}$$

In the high energy case, Equation 8, the decrease in velocity $\Delta\beta$ is roughly proportional to the change in radius Δr (the sign of μ properly accounting for inward or outward propagation). On the other hand, in the low energy case, Equation 9, the field-aligned motion of the particle contributes little compared to the convection of the field line radially outward at the solar wind velocity. The particle is swept outward (even though its parallel velocity may be inward) and it 'cools' as a power-law in distance. In the isotropic case we described under Eq. 5, where $(1/2)\mathrm{d}\ln T/\mathrm{d}t = -2V/3r$ so that $F = 2/3$, we recover the well-known 'adiabatic cooling' law $v \propto r^{-2/3}$ or $T \propto r^{-4/3}$. To reiterate an essential point: the results of these estimations depended only on the initial positions and velocities of the particles, but not on their mass or their charge. The results hold for all species and charge states of ions, as well as for electrons.

3.3. Random Connection – Perpendicular Diffusion

J. KÓTA and J. R. JOKIPII

As mentioned in the previous paragraphs, adiabatic cooling occurs even for scatter-free transport; curvature drifts move the particles against the $\mathbf{V}\times\mathbf{B}$ electric field.

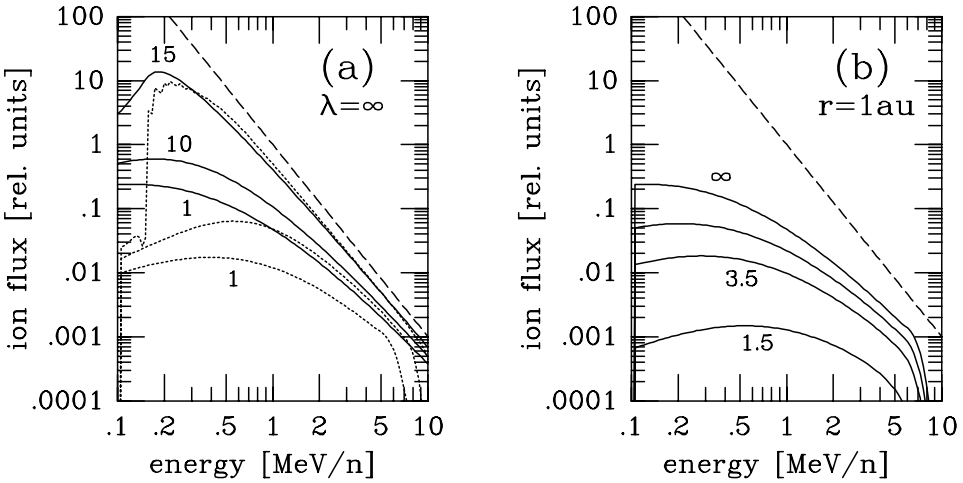

Figure 8. Energy spectra at 1, 10, and 15 AU obtained from a spectrum imposed at 15 AU (dashed line). The left panel shows scatter-free propagation (solid lines) and hemispherical scattering (dotted lines). The right panel shows the resulting spectra at 1 AU for the mean free path values of ∞, 7, 3.5, and 1.5 AU.

The transit time and thus the net cooling and reduction of flux can increase by a significant factor if scattering is not negligible. The transport of energetic particles, including convection, adiabatic focusing, cooling or acceleration, and random pitch-angle scattering, is described by a Fokker-Planck equation, which is equally applicable for low or high rates of scattering (Skilling, 1971; Isenberg, 1997; Kóta and Jokipii, 1997).

Figure 8 shows some illustrative examples on the reduction of ion fluxes due to adiabatic cooling when scattering is included. An E^{-3} spectrum is imposed at 30^o latitude, 15 AU from the Sun to represent CIR-accelerated particles, then the distribution resulting along the spiral field line is computed. The left panel (a) shows the spectra obtained for scatter-free propagation (solid lines) and for strong hemispherical scattering, with no scattering through $\mu = 0$ (dotted lines), respectively. Substantial modulation occurs in both cases. Standard diffusion models, which would give $\kappa_{\|} \to \infty$ and no modulation, are inapplicable to these cases. Hemispherical scattering, which corresponds to an effective speed of half the particle speed along the field line, results in longer transit times, and larger modulation. Figure 8a also indicates that most of the cooling and flux reduction takes place between 10 and 15 AU, where field lines are more tightly wound.

The right panel (b) shows the resulting spectra at 1 AU for various scattering mean free paths, λ. $\lambda = 1.5$ AU results already in a $\sim 10^4$ factor of reduction.

This adiabatic cooling may account for the decrease of the magnitude of ion events at high latitudes (Simnett *et al.*, 1995a; Sanderson *et al.*, 1995). At the same time, these considerations may set a lower limit for the scattering mean free path and/or an upper limit for the heliocentric radius of the CIR where acceleration takes place.

The same rate of adiabatic cooling, averaged over pitch angles, appears in Parker's equation if particle transport is diffusive. Diffusion across the mean field may shorten the path particles have to travel. Also, connection to CIRs closer than 15 AU may become possible if random walk of the field lines is significant.

The continued appearence of low-energy ion and electron events at high latitudes can be understood in terms of random latitudinal transport due to the random walk of field lines (which does not exclude the possibility of an additional organized latitudinal motion). Figure 9 shows the results of a model simulation (Kóta and Jokipii, 1998) for ~ 0.7 MeV protons and ~ 70 keV electrons, assuming considerable perpendicular diffusion ($\kappa_\perp/\kappa_\parallel$ in the 0.02–0.05 range). Accelerated spectra of ions and electrons are imposed as sources at shocks and compression regions, then the transport of these particle populations is followed in the simulation, including convection, diffusion, drifts and further acceleration or deceleration. Results indicate that, for reasonable values of perpendicular diffusion, low-energy CIR-accelerated particles can be expected to appear at high heliographic latitudes. The effect is more pronounced if perpendicular diffusion is enhanced in the latitudinal direction as suggested by Jokipii (1973).

The lower panel of Fig. 9 indicates that the phase shift between the ion and electron events observed by Ulysses at high latitudes (Simnett *et al.*, 1995a; Simnett and Roelof, 1997) is a natural consequence of the model. Slow ions are effectively convected outward by the solar wind, thus only the ions accelerated close to the Sun are able to reach Ulysses at high latitudes; this results in peaked events with diminishing magnitudes. Electrons, on the other hand, are mobile and can reach Ulysses from a larger area, which explains their longer duration in time. The time lag may be interpreted in terms of a velocity shear between lower and higher latitudes (Kóta and Jokipii, 1998).

3.4. Random-Phased Wavy Spiral Magnetic Fields in Space

Y.-Q. LOU

Ulysses observations revealed a remarkable fact that periodic solar modulation ($\sim$26 days) of cosmic rays and energetic particles accelerated by CIR shocks at low latitudes (within $\pm 35^\circ$) in the magnetized solar wind *persist* to high heliographic latitudes with decreasing strengths (Simpson *et al.*, 1995; Keppler *et al.*, 1995; Lanzerotti *et al.*, 1995). Two immediate questions come to mind. First, why should cosmic ray fluxes at high latitudes be modulated by low-latitude CIR shocks? Second, how do energetic particles accelerated by CIR shocks reach higher latitudes, given a mean spiral magnetic field in the heliosphere? Here, we present a scenario of random-phased wavy spiral magnetic fields (over a wide frequency range) in the solar wind (see Fig. 10 and Lou, 1996) and explain in physical terms how *global* solar modulation of cosmic rays and energetic particles works. For a detailed analysis of wavy spiral magnetic fields, one is referred to Lou (1994) on Alfvénic fluctuations in the solar wind with a mean spiral magnetic field.

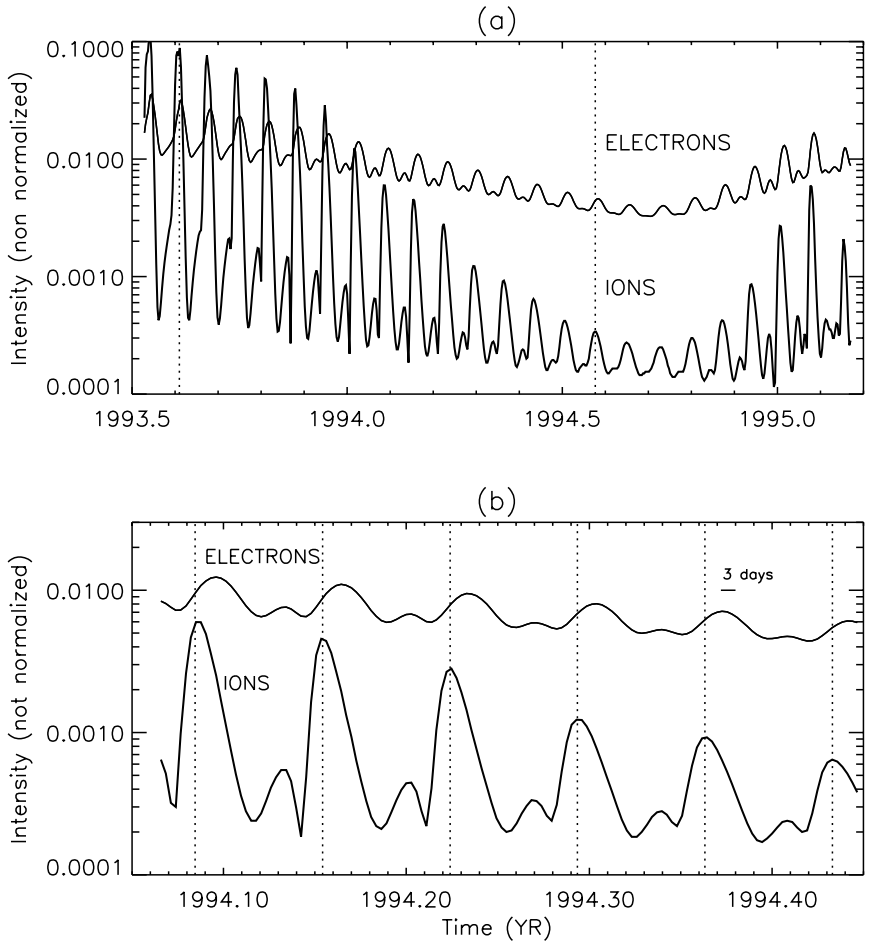

Figure 9. Simulated variations of ~ 0.7 MeV proton and ~ 70 keV electron fluxes along the trajectory of Ulysses around the southern polar pass. The lower panel shows a shorter period in early 1994 to emphasize the phase shift between electrons and ions. A dash in the bottom panel is to indicate a 3-day period.

Ulysses observations (Balogh *et al.*, 1995b) confirmed the ubiquitous presence of random fluctuations of large-amplitude transverse magnetic field in the polar heliosphere (Jokipii and Kóta, 1989; Hollweg and Lee, 1989; Roberts, 1990; Lou, 1992; 1993) and, as a result, the more or less *isotropic* distribution of the mean cosmic ray flux intensity in the heliosphere (Simpson *et al.*, 1995). Given this overall isotropic cosmic ray flux, one can see consequences of CIR shocks. As a spacecraft is submerged *inside* a CIR shock, much enhanced magnetic fields therein bend and shield off cosmic rays to yield a much reduced flux intensity. At a higher latitude just outside a CIR, the spatial extent of the CIR subtends a huge solid angle (nearly a half space) towards a spacecraft; the spacecraft still receives a

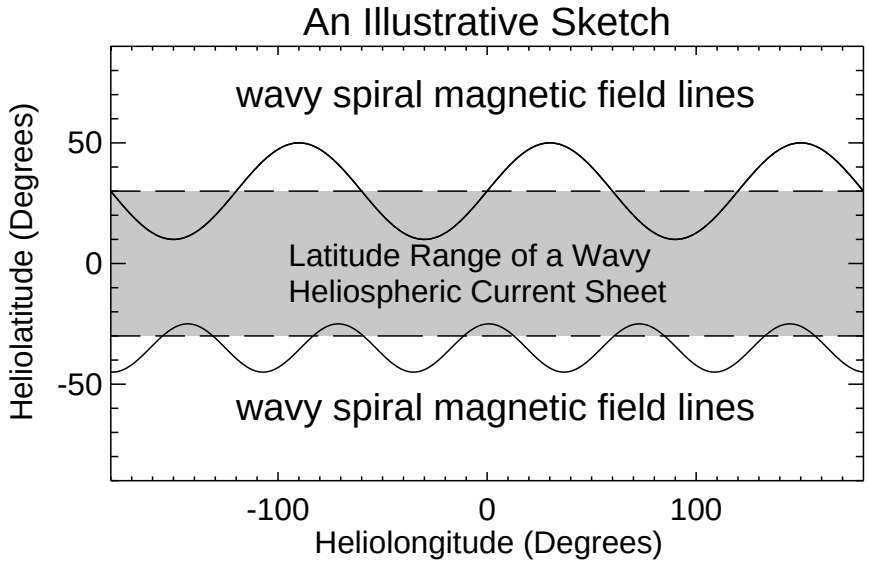

Figure 10. Schematic illustration of latitude excursions of wavy spiral magnetic fieldlines in relation to heliospheric current sheet latitude extent.

significantly reduced cosmic ray flux. As a spacecraft ascends to higher latitudes, low-latitude CIRs subtend smaller solid angles towards the spacecraft and thus CIR modulations of cosmic rays become progressively weaker.

As shown in Fig. 10, it is possible for an individual large-amplitude wavy spiral magnetic field line to directly connect high- and low-latitude regions. When lower portions of a magnetic field line dip into low-latitude CIRs, shock-accelerated energetic particles can readily climb up to higher latitudes. For an ensemble of wavy spiral magnetic field lines in interplanetary space, one would expect a random distribution in space and time of phases and amplitudes among individual wavy magnetic field lines. In this manner, energetic particles generated by CIR shocks can propagate to higher heliographic latitudes more or less following the solar modulation period of $\sim$26 days (Keppler *et al.*, 1995; Lanzerotti *et al.*, 1995). Meanwhile, cross-field diffusion should be effectively enhanced as a result of randomness (Kóta and Jokipii, 1995). This naturally explains why modulation of cosmic rays and energetic particles should anticorrelate with each other at all latitudes. Since Alfvénic fluctuations are transverse and incompressible, wavy spiral magnetic fields will not produce conspicuous compressions in the persistently fast polar solar wind and the wind advects these fluctuations radially outward. In the above description, the presence of a randomly fluctuating spiral magnetic field in space is essential.

As to the origin of random fluctuations of transverse magnetic fields in the solar wind, there are several possible sources. Granule and supergranule motions over the solar surface can give rise to wave fluctuations (Jokipii and Kóta, 1989) with

time scales ranging from minutes to days. Energetic events, such as coronal mass ejections and solar flares, and the opening of closed magnetic field regions can certainly produce magnetic field fluctuations in the solar wind (Reiner *et al.*, 1995). Here, we emphasize that the interfaces at $\sim \pm 35^{\circ}$ between the persistently fast polar solar wind ($\sim$700 km/s) and the low-latitude periodically varying solar wind embedded with CIRs will inevitably suffer Kelvin-Helmholtz (KH) instabilities (*cf.* Chandrasekhar, 1961). The mean spiral magnetic field is roughly perpendicular to the radial solar wind and thus cannot suppress such KH instabilities. As a result, large-amplitude Alfvénic fluctuations with low frequencies and long azimuthal wavelengths in spiral magnetic fields can be sustained along the interfaces by periodically varying shears in solar wind speeds (Lou, 1996). In particular, magnetic field fluctuations should be stronger along those portions associated with CIRs because of stronger shears.

4. Comparison of the CIRs Observed by Ulysses in the Southern and Northern Heliosphere

4.1. The Influence of the Current Sheet on the Recurrence of CIRs at 4–5 AU

T. R. SANDERSON and R. J. FORSYTH

4.1.1. *Introduction*

The evolution of the Sun's neutral sheet and its influence on the interplanetary medium has been the subject of continual attention for at least the last two solar cycles, ever since the first attempts to measure and quantify its position. Measurements on IMP 1 as early as 1965 (Wilcox and Ness, 1965) had shown the existence of magnetic sectors of opposite polarity in the interplanetary magnetic field at 1 AU. To explain this, Schatten *et al.* (1969) used a mathematical model of a spherical source surface and a radially emanating field, with a neutral line separating the two hemispheres and related it to the interplanetary magnetic field sector boundaries.

Schulz (1973) suggested that these magnetic sectors were the result of multiple crossings of the large-scale heliospheric current sheet separating two opposite hemispheres of the Sun. The 2-sector patterns were the result of a tilted solar magnetic dipole, and the 4-sector patterns were the result of an additional warp due to a quadrupole contribution to the current sheet.

Since then there have been numerous attempts to relate measurements on the Sun to observations at 1 AU. Of relevance here are the early works describing solar minimum 2 solar cycles ago, *e.g.* Burlaga *et al.* (1981) and Hoeksema *et al.* (1982; 1983), which established and quantified many of the ideas presented in this paper. These authors, using either K-Coronameter or Solar Heliograph measurements, found that at solar minimum the tilt of the dipole is small, typically only a few

degrees, and that small warps of only a few degrees can be as significant as the tilt. In the period around solar minimum two solar cycles ago (Hoeksema *et al.*, 1982), the warp and the tilt were such that two northward and two southward extensions of the current sheet were observed, giving rise to a 4-sector structure at 1 AU. The general trend was that of a slow evolution of features affecting the current sheet with a time scale of several months, different features drifting slowly either east- or westwards relative to the coronal rotation, similar to the observations which we will present here.

In recent years, the Ulysses mission has enabled us to look at the interaction regions caused by a tilted current sheet and their effect on energetic particles. Smith *et al.* (1993) showed that between 13° S and 29° S, 4 interaction regions per rotation were observed. According to Sanderson *et al.* (1994) and Simnett *et al.* (1994) these interaction regions were responsible for the acceleration of the observed energetic particles.

The formation of these interaction regions has been explained by Gosling *et al.* (1993). In their model a band of slow solar wind from the coronal streamer belt, tilted at an angle relative to the solar equator, is surrounded by fast solar wind flow from the polar coronal holes. The tilt is caused by the tilt of the magnetic dipole relative to the solar rotation axis and changes with different phases of the solar cycle. Fast solar wind overtakes the slow solar wind far from the Sun along interfaces that are inclined relative to the equator in the same sense as the original belt of slow wind, creating an interaction region. Forward and reverse waves propagate perpendicular to this interaction region, the forward wave into the slow solar wind (and hence to low latitudes), and the reverse wave into the fast solar wind (and hence to high latitudes). This explanation used the modelling of Pizzo and Gosling (1994) of corotating flows originating in a tilted dipole geometry back at the Sun.

4.1.2. *Summary of the Ulysses Mission*

Figure 11, from Sanderson *et al.* (1999), is a summary of observations for the first complete orbit of the Ulysses spacecraft around the Sun. The top panel shows 1.2–3.0 MeV proton and 8.4–19 MeV/amu α-particle intensities. The next panel shows the solar wind speed. The bottom panel shows the locus of the neutral line as measured on the Sun by the Wilcox Solar Observatory Solar Magnetograph and the heliographic latitude of the spacecraft. The most interesting periods, from the particle acceleration point of view, were the two $\sim$1-year periods when the spacecraft passed from the slow solar wind of the streamer belt to the high-speed solar wind flow of the polar coronal hole, and back, every solar rotation. These two periods, labeled 1 and 2 in Fig. 11, lasted from mid-1992 to mid-1993 (Period 1) and from late-1996 to mid-1997 (Period 2). During these times regular recurrent increases of locally accelerated particles were observed. The much shorter fast latitude scan, which has already been discussed earlier (Sanderson *et al.*, 1996), will not be discussed in detail here.

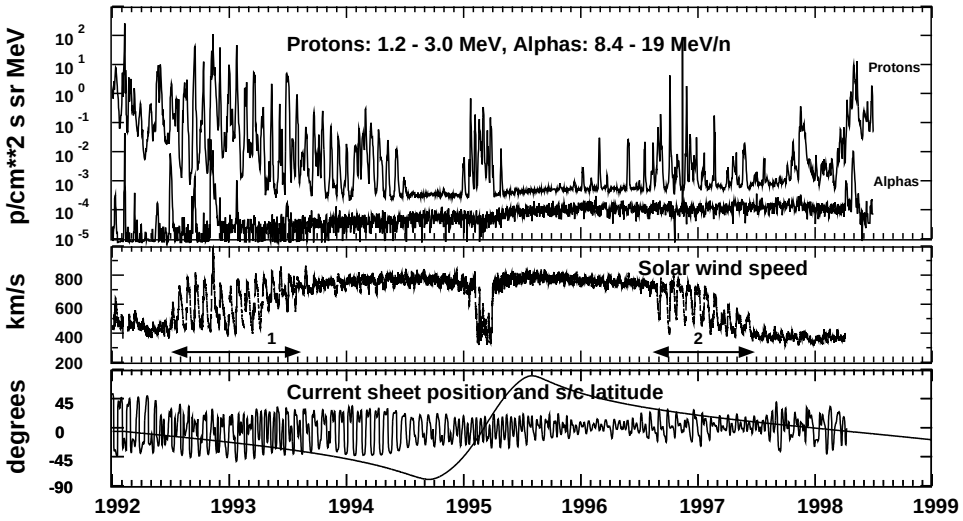

Figure 11. Summary plot of Ulysses' first out-of-ecliptic orbit showing proton and α-particle intensity, solar wind speed, position of the current sheet at the Sun, and spacecraft heliographic latitude.

4.1.3. *Southern Polar Pass*

In 1992, Ulysses was slowly moving to higher southern latitudes, and crossing the tilted current sheet at least once per solar rotation, as can be seen in Fig. 11. In mid-1992, at the start of Period 1, a major re-organisation of the solar coronal fields changed the shape of the current sheet, giving rise to a new 2-sector interplanetary magnetic field structure, as reported by Balogh *et al.* (1993). One major high-speed stream was observed coming from the southern hemisphere, its appearance being attributed by Bame *et al.* (1993) to the equatorward extension of the coronal hole.

Figure 12 shows data for 12 solar rotations during Period 1, starting on 12 January 1993, taken from Sanderson *et al.* (1999). This includes 5 of the 6 solar rotations studied by Smith *et al.* (1993), labeled here numbers 9–13. During the first 4 rotations shown here, 4 interaction regions per rotation were observed, which Smith *et al.* (1993) labeled **a, b, c** and **d**. Three of these, **a, b** and **d**, originated from the southern hemisphere, whilst the other, **c**, originated from the northern hemisphere. These interaction regions were associated with forward or reverse shocks, or even forward-reverse shock pairs.

The thick bar shows the point where the current sheet crosses over the position of the spacecraft, following the model of Gosling *et al.* (1993), as the possible location on the current sheet which should correspond to the interaction regions of Smith *et al.* (1993).

At the start of the period shown in Fig. 12, in rotation 9, Ulysses crossed over the current sheet once per rotation, and one dominant interaction region, labeled **d**, was observed. The black bar shows the expected position of the corresponding interaction regions. The main particle intensity increase was observed at the trailing edge of interaction region **d**, where a reverse shock was observed.

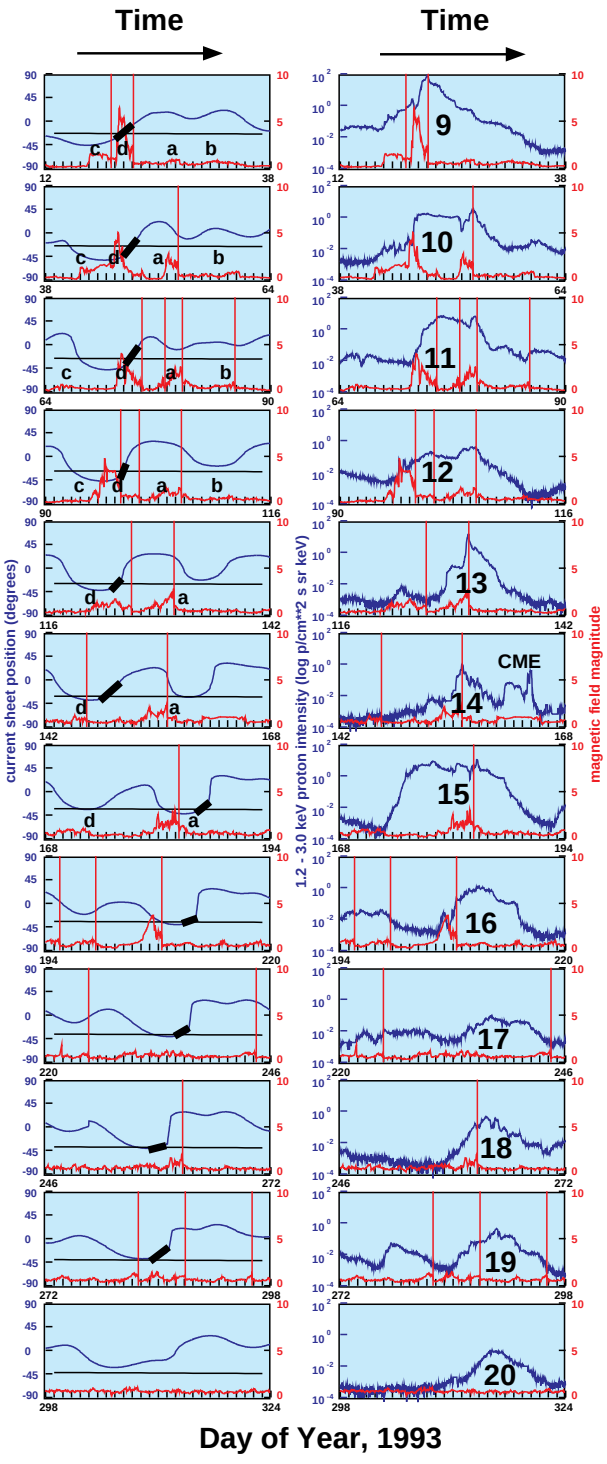

Figure 12. Data from 12 solar rotations, each of 26 days, starting on 12 January 1993. Time runs from left to right. The left column shows, in blue, the expected latitude of the current sheet at the position of the spacecraft. The black trace shows the position of the spacecraft, while the red trace shows the magnitude of the magnetic field. The right column shows, in blue, the 1.8–3.8 MeV proton intensity. The vertical lines show the observed times of reverse shocks, whilst the solid bars show the expected positions of the interaction regions using the model of Gosling *et al.* (1993).

During rotations 9–13, interaction region **d** slowly diminished in strength. Interaction region **a**, due to a new warp in the current sheet that developed north of Ulysses, slowly increased in strength. By rotation 15, a substantial warp, shown by the second thick bar, had developed, which then continued to dominate the shape of the current sheet. The smaller peak in the particle intensity, which was associated with interaction region **a**, slowly grew in importance until by rotation 15, the major particle intensity peak was at region **a** instead of **d** (Sanderson *et al.*, 1994). During rotation 20, a peak in the particle intensity was observed even though the spacecraft was no longer crossing the current sheet, and no reverse shock was observed. The particle intensity profile was now much more rounded, and was most likely due to an acceleration process taking place further away from the spacecraft.

When the new warp first appeared (rotation 13) it did not coincide exactly in time with interaction region **a**. At this time the spacecraft was above the current sheet, so that the connection to the interaction region was probably longer than the distance from the Sun to the spacecraft. However, the general trend of a change in position of the relevant warp in the current sheet fits the overall pattern of the observed recurrences.

The change-over in importance of interaction region **d** to **a** gave the illusion of a change of phase of the particle intensity peak, which could be taken as a periodicity different from the ∼26-day periodicity observed for the individual interaction regions.

No evidence was found for any major deviation from the ∼26-day periodicity, other than small drifts east- or westwards of the interaction regions due to the movement of the Sun's active regions, such as was found by Hoeksema *et al.* (1982).

4.1.4. *Northern Polar Pass*

Figure 13, taken from Sanderson *et al.* (1999), shows the return from the northern polar regions to the ecliptic as the spacecraft passed from complete immersion in high-speed flow to immersion in the low-speed flow of the streamer belt (McComas *et al.*, 1998).

At the start of 1996, particle increases began to be seen again as Ulysses was descending towards the current sheet after the northern polar pass. Several increases were observed during the first half of 1996 whilst Ulysses was still completely immersed in high-speed flow, despite the lack of any interaction regions. Similar observations of this period by Roelof *et al.* (1997) are included in Sect. 4.3.

The first four peaks of 1996 were observed with a period of around ∼26 days. New peaks, with a different phase but still with period ∼26 days, were observed starting at the end of May 1996, again with no significant interaction regions. The first encounter with lower speed flow started around 1 October (Gosling *et al.*, 1997). Thereafter, 11 excursions in and out of the low-speed flow were observed, labeled 1 to 11 in reverse order, following the convention used by Bame *et al.* (1993) for numbering the peaks during 1992–1993. This culminated in complete immersion in the slow speed flow of ∼375 km/s in mid-1997.

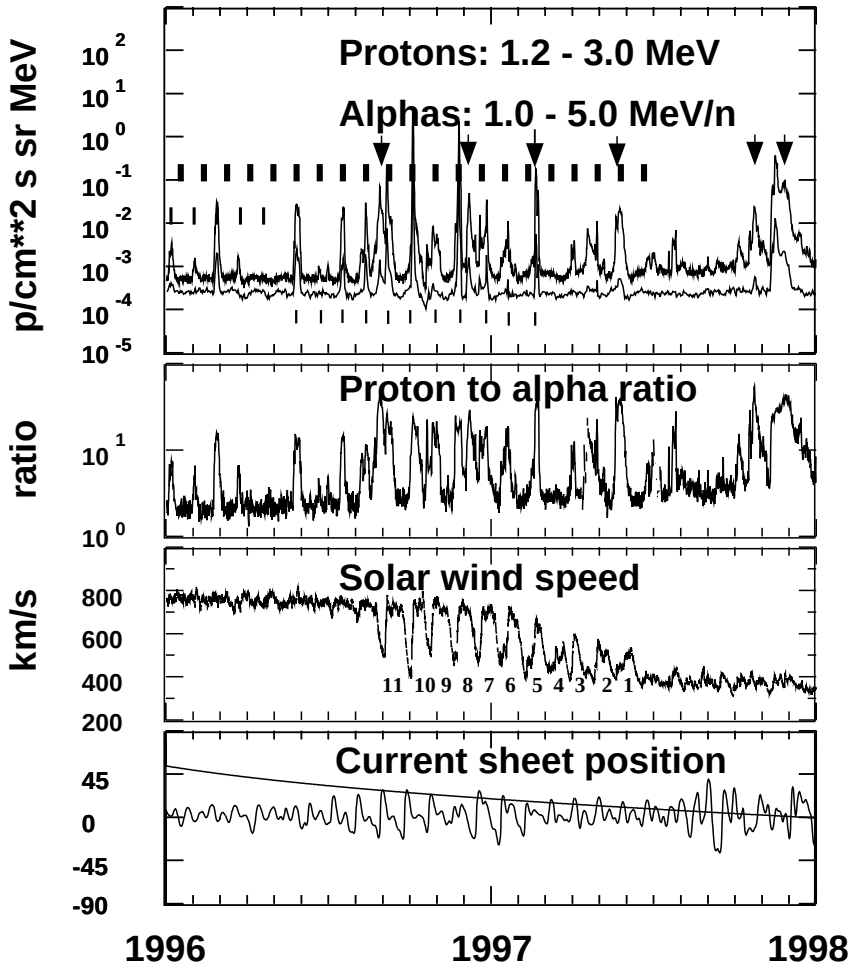

Figure 13. The return to the ecliptic as observed in 1996 and 1997. The top panel shows the 1.2–3.0 MeV proton and the 1.0–5.0 MeV α-particle intensity. The next panel shows the proton to alpha ratio at around 1 MeV. (Disregard quiet time values because of background.) The next panel shows the solar wind speed, whilst the bottom panel shows the current sheet position at the Sun together with the heliographic position of the spacecraft. The vertical arrows show the times of transient events. The vertical bars are spaced 26 days apart.

Associated with these transitions was a regular pattern of particle increases, interspersed within which were several transient events. In Fig. 13 vertical arrows show the times of the transient events. The transient events can easily be identified by their somewhat higher (∼50–80) proton to α-particle abundance ratio than the CIR events. Thin vertical bars spaced every 25.6 days are included to show the regularity of the first 4 peaks, and thick vertical bars with a different phase to show periodicity of the other peaks.

During all this time, the latitude of the spacecraft was slowly decreasing, reaching in September 1996 the position of the current sheet, as projected out to the position of the spacecraft (Forsyth *et al.*, 1997). Low-speed flow of around 400 km/s was encountered on around 1 October 1996, but the spacecraft never really entered the 400 km/s flow again until February 1997. Ulysses finally entered full immersion in slow speed flow in July 1997, the slow decrease in the northern extension of the current sheet just about matching the decrease in latitude of the orbital position. The spacecraft only just entered the low-speed flow, with the current sheet retreating at about the same rate as the spacecraft approached it.

Figure 14 shows data for the 16 rotations starting on 1 January 1996, rotations 5–20. In the first 4 rotations, 20, 19, 18 and 17, peaks in the particle intensity can be observed recurring with a periodicity of around 26 days. Ulysses was far from the current sheet at this time and not encountering the local interaction regions, and so these particles must have been accelerated at some remote site. These particle increases, with rounded intensity-time profiles, are typical of the increases observed when no local shock or compression region was seen. The solid red bars show the possible location of the interaction regions far away from the spacecraft.

In rotation 15, a new peak in the particle intensity appears, but at a different phase, coincident with a change in the shape of the current sheet. At this time, a new warp in the current sheet appeared, shown with a second bar, increasing in strength and dominating the shape of the current sheet over the remaining 11 rotations shown in Fig. 14.

The spacecraft entered the low-speed flow around rotation 11, and interaction regions started to appear, as did forward and reverse shocks and the associated peaks in the particle increases. During rotations 15 down to 6, the particle increases stayed at approximately the same phase, implying a periodicity of $\sim$26 days, the pattern of increases following closely the crossing of the current sheet.

Again, no evidence was found for any periodicity other than the $\sim$26 day period seen in the southern pass. Rather, an evolution of the current sheet on the Sun which, just like the observation in Period 1, controls the recurrence of the interaction regions and hence the peaks in the particle intensity profiles.

The particle profiles associated with streams 13 to 20 are typical of those observed when no shocks are seen, *i.e.* somewhat rounded, and lasting for several days (Sanderson *et al.*, 1994). Those associated with rotations 6 to 12 are typical of those associated with shocks, with the particle intensity more spiky and a sharp peak at the shock.

These observations show how the neutral line observed on the Sun, when projected to the position of Ulysses using a simple approximation, can be used to predict the position of the current sheet at the spacecraft. Using the model of Gosling *et al.* (1997) we can determine the position of the interaction regions formed by the interaction of the high-speed polar coronal flow with low-speed streamer belt flow. Since these interaction regions are responsible for the acceleration of the energetic particles in the CIRs, one can predict the pattern of the particle increases.

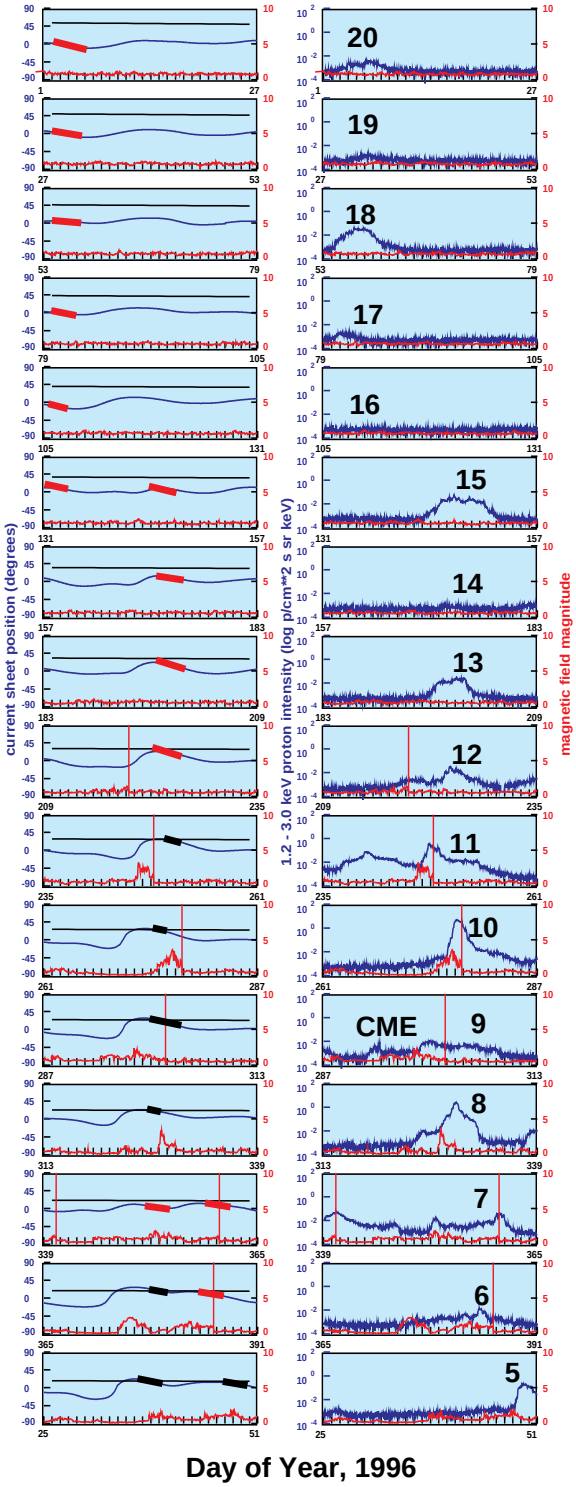

Figure 14. Data from 16 solar rotations starting on 1 January 1996. The left column shows the expected latitude of the current sheet at the position of the spacecraft. The solid, almost horizontal line shows the position of the spacecraft. The right hand side shows the 1.8–3.8 MeV proton intensity. The vertical lines show the observed times of reverse shocks, whilst the solid bars show the expected positions of the interaction regions using the model of Gosling *et al.* (1993).

4.1.5. *Summary*

During the passage from the ecliptic to southern latitudes, the spacecraft crossed the current sheet only once per rotation, despite the fact that the sheet had an almost sinusoidal form with a period of around half a solar rotation. This shape was due to a warp in the current sheet that had the right phase and amplitude to change the otherwise flat but tilted current sheet into this shape. At Ulysses, a 2-sector structure was observed, with four interaction regions per rotation, with a mix of forward and reverse shocks, and a compound high-speed flow structure. A very regular pattern of particle increases was observed, with a broad particle increase per rotation, one dominant peak, and the phase changing very slowly as the dominance of one interaction region took over from another.

A completely different current sheet was observed during the passage from northern latitudes back to the ecliptic. A differently shaped and phased warp and a smaller dipole tilt gave rise to an asymmetric two-sector structure at Ulysses with the spacecraft staying in the northern hemisphere for about twice as long as in the southern hemisphere. A regular pattern of particle increases was seen. In May 1996, a dramatic change in the shape of the current sheet changed the phase of the increases, when, just like during the first period, one interaction region took over in importance from the other, changing dramatically the phasing of the particle increases.

The observations were made under widely differing conditions. Period 1, the ascent to high southern latitudes was in solar cycle 22 when the dipole tilt was large, whilst Period 2, the return to low latitudes was during the early phase of solar cycle 23 when the dipole tilt was small. Nevertheless we observe the same features in both periods. Interaction regions, coming from the interaction of the high-speed streams with the low-speed streams propagate past the spacecraft, as in the model of Gosling *et al.* (1993). The timing and strength of these interaction regions changes as the dipole tilt changes, as the warps in the current sheet slowly change in amplitude, and as the position of the spacecraft changes relative to the current sheet. This is followed by corresponding changes in the phase and amplitude of the peaks in the particle intensity profiles, which give rise to the pattern of particle increases seen at Ulysses.

4.2. Current Sheet Structure During the Northern CIR

R. J. FORSYTH

During 1996 solar activity, as measured by monthly mean Sunspot number, was low and should be close to minimum. It was certainly lower than in March 1995 (at the time of the Ulysses fast latitude scan), and in the most recent Sunspot number data (Solar Geophysical Data, April 1997, Pt. 1) there is no evidence of any rise in mid-1996 or more recently. Thus, in principle, there would be no reason to expect that the HCS tilt during 1996 would be any greater than that observed by Ulysses in 1995.

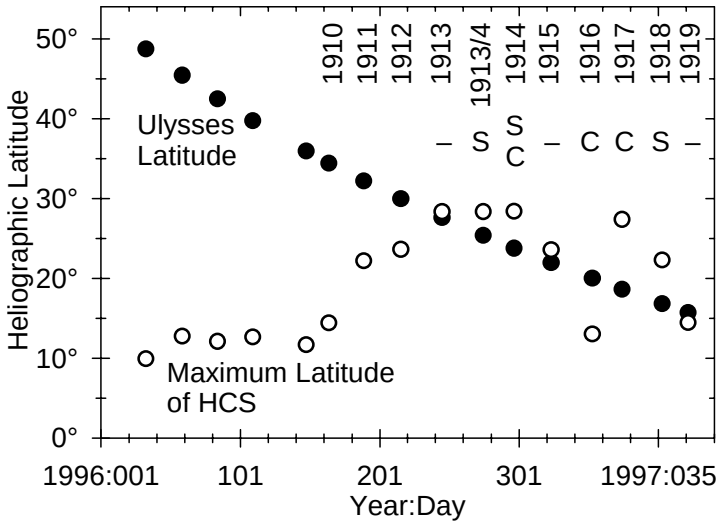

Figure 15. A comparison of the latitude of Ulysses with the maximum latitude of the HCS deduced from the neutral line at the source surface. The annotation is described in the text.

To gain a first understanding of how the HCS behaviour at this time is related to the structure of the solar corona, we have compared the Ulysses HCS data with the neutral line on the Stanford University source surface maps, available via the Stanford web site or in Solar Geophysical Data. These maps are produced (*e.g.* Hoeksema, 1995) by extrapolating outwards the photospheric magnetic fields measured at the Wilcox Solar Observatory (WSO) using a potential field model with an outer boundary condition that the magnetic field lines are all open and radial at 2.5 solar radii from the Sun, the so-called 'source surface'. Magnetic fields originating from the northern and southern hemispheres are separated by the neutral line at the source surface, and thus the HCS observed at Ulysses should map back to the neutral line. One synoptic map is produced per Carrington Rotation as the Sun rotates as seen from Earth.

For each of the Carrington rotations in Fig. 14 we determined the maximum heliographic latitude reached by the neutral line and the Carrington longitude at which this occurred. The results are shown in Fig. 15. The maximum latitude of the HCS and the latitude of Ulysses are plotted at the time that a parcel of plasma emitted from the appropriate longitude would reach Ulysses. To aid comparison with Fig. 14, the Carrington Rotation numbers corresponding to each data point are shown along the top of the figure. Beneath these, the letter S indicates that a magnetic field sector was observed and C indicates that a CME was observed during the rotation; all three CMEs were seen near longitudes where we might have expected to observe sector boundaries.

Figure 15 shows that the reappearance of magnetic field sector structure at Ulysses in September 1996 was a combination of the steadily reducing latitude

of Ulysses and a rapid rise in the maximum latitude of the HCS deduced from the source surface maps. The rise started around June 1996 in the interval comparable with CR1910. In the interval covered by CR1915 the predicted maximum HCS latitude drops again slightly and the lack of a clear sector boundary at Ulysses is consistent with the spacecraft having a similar latitude. Skipping CR1916 and 1917 where the issue is confused by the CME signatures, we find that the sector in CR1918 is correctly predicted and also the absence in CR1919. Where sectors are observed at Ulysses, the estimated source longitude is consistent with the longitude of the maximum latitude of the neutral line. For CR1910-1915 this is within $\pm 10^\circ$ of 240° Carrington longitude. Thus, this study provides a further confirmation that the neutral line on the Stanford source surface maps provide a first order prediction of where HCS crossings will be observed by Ulysses. Preliminary comparisons with HCS maximum latitudes deduced from SOHO/LASCO synoptic maps (Y.-M. Wang and R. A. Howard, personal communication) suggest lower maximum latitudes than obtained from the Stanford maps, but with least disagreement ($\sim 3^\circ$) in CR1913–1914 when Ulysses re-encountered the HCS, and thus not inconsistent with our observations. It is also noted that the alternative Stanford source surface maps, produced assuming the photospheric fields are purely radial and placing the source surface at 3.25 solar radii, also suggest lower maximum latitudes for the neutral line. However, these completely fail to predict the higher latitude Ulysses HCS crossings, most likely due to the source surface being set too high. This alternative model is apparently more successful at 1 AU near the ecliptic, and agreed better with the latitude of the first Ulysses southward crossing in 1993 (Phillips *et al.*, 1994).

We have presented observations showing the reappearance of the magnetic field compressions associated with CIRs and the reappearance of magnetic field sector structure at Ulysses as the spacecraft returned from high northern latitudes. The maximum northern latitude reached by the HCS, as observed by Ulysses on 30 Sept. 1996, was 25.5° N. This is a significantly higher latitude than that inferred from the Ulysses fast latitude scan observations in 1995, and given the lower solar activity in 1996 as discussed in the introduction, this higher maximum latitude is at first surprising. Thus it is interesting to ask what change in the photosphere and/or corona caused the latitude rise of the neutral line shown in Fig. 15 and hence the reappearance of HCS crossings at Ulysses. In an attempt to address this, Figure 16 shows a Carrington map of the photospheric magnetic field measured at WSO for CR1913. The solid lines represent contours of zero and increasingly positive (or outward) magnetic field strength and the dashed lines represent contours of increasingly negative (or inward) field strength. The map, derived from a sequence of full disk magnetograms, forms the inner boundary condition in the calculation of the source surface maps to which we compared the Ulysses HCS observations. The neutral line thus calculated for CR1913 at the 2.5 solar radii source surface has been overlaid on Fig. 16 as a heavy black line. A strong bipolar feature, characteristic of an active region, is clear in the photospheric field at this time, in the longitude range

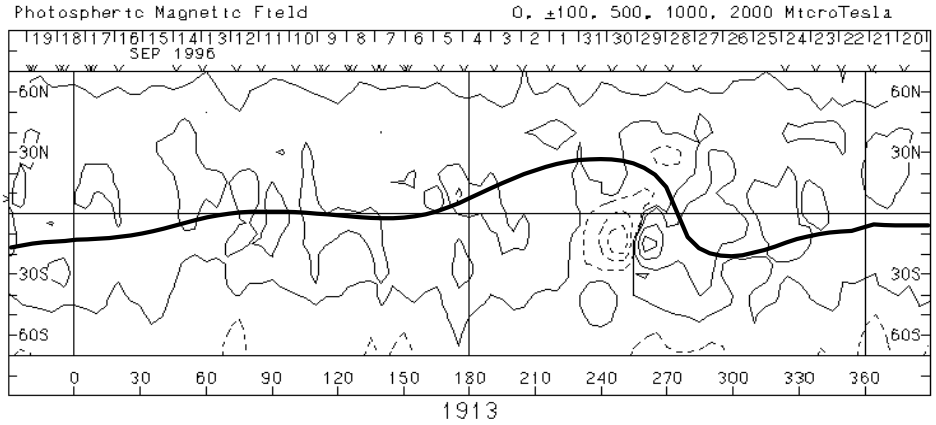

Figure 16. A Carrington map of the photospheric magnetic field observed by Wilcox Solar Observatory for Carrington Rotation 1913. Note the bipolar signature of the active region near 240° longitude. The heavier overlaid black line shows the location of the neutral line at the source surface.

230–270°. Its negative polarity region is centred on 240° longitude and extends to high northern latitudes, consistent with the longitude where Ulysses observed negative polarity. Inspection of a sequence of these synoptic maps shows that this feature was present from CR1910 to CR1915, being most pronounced in 1912–14. The associated active region was visible in YOHKOH/SXT (Solar Geophysical Data, 1996) and SOHO/EIT images (B. J. Thompson, personal communication) over approximately the same period.

Thus a reasonable interpretation would be that this long-lived active region was responsible for producing the strong northward deflection of the HCS localised at Carrington longitude 240°, leading to its earlier and higher latitude than expected observation at Ulysses. This conclusion is supported by the recent coronal field modeling work of Wang *et al.* (1997) based on SOHO-LASCO coronagraph observations from the same time period.

4.3. Electron and Proton Intensity Increases in the Northern Hemisphere

G. M. Simnett, E. C. Roelof, and B. Heber

One of the features of the Ulysses high-latitude pass in the southern hemisphere was the occurrence of periodic increases in the intensities of both ions up to a few MeV/amu and mildly relativistic electrons. At the same time the intensity of galactic cosmic rays showed periodic decreases. The appearance of recurrent ∼50 keV electron events continued right up to 80° latitude. When taken together, these phenomena have been interpreted as evidence for a remote magnetic connection to a low-latitude CIR at a distant radial distance from Ulysses (Fisk, 1996). With Fisk's interpretation the solar magnetic field undergoes significant latitudinal

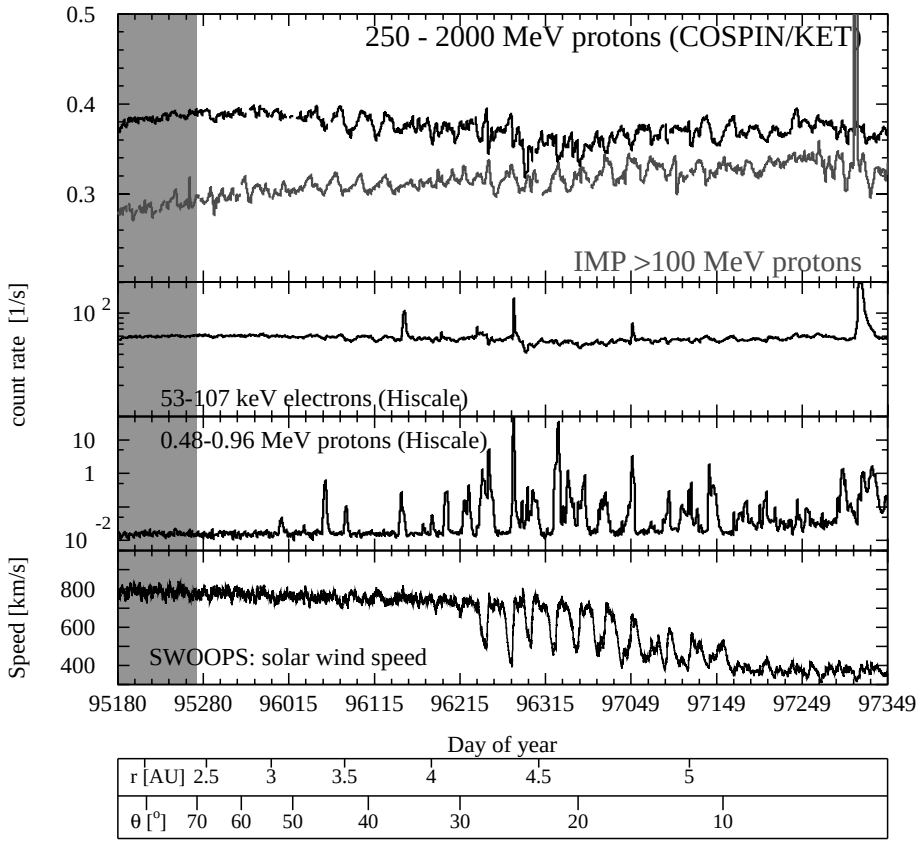

Figure 17. Energetic particles observed during the northern pass of Ulysses (heliolatitude and radial distance are shown at the foot of the figure): 250–2000 MeV protons together with >100 MeV protons from IMP 8, 53–107 keV electron and 0.48–0.96 MeV proton intensities. The bottom panel shows the solar wind speed.

fluctuations such that particles accelerated by a CIR at a radial distance considerably beyond Ulysses might gain access to field lines passing through Ulysses. The CIR structure is also responsible for modulating the ingress of galactic cosmic rays, which shows up as a minimum at the same time as the CIR-accelerated particles show a maximum. It is of interest to understand whether these particle increases and the galactic cosmic ray modulation are a function of latitude only, or whether they are critically dependent on the nature of the high-speed solar wind stream responsible for the CIRs. In the latter case they would be solar-cycle dependent. Detailed analysis of the electron/proton ratio and the electron and proton spectra should also provide revealing information on the nature of the acceleration processes occurring in the interplanetary medium. A summary of these data may be found in Simnett *et al.* (1998) in their Figs. 1–3 and Heber *et al.* (1997).

We have now extended the analysis to include the whole of the Ulysses descent to the ecliptic plane, and Fig. 17 shows the higher energy particle data from

COSPIN, together with the >100 MeV proton intensity from IMP 8. The middle panels show the 53–107 keV electron and 0.48–0.96 MeV proton intensities from HI-SCALE, although there are only a few occasions when the electron intensity is above background. This is rather different from the southern hemisphere pass, when proton increases were seen up to $\sim 65^\circ$ and low energy electron increases up to 80°. The bottom panel shows the SWOOPS solar wind speed. Comparison of the lower two panels shows that the amplitude of the proton increases is largest when the 26-day modulation of the solar wind speed is largest.

Simnett and Roelof (1997) showed that as Ulysses went over the northern solar polar region and started its descent to lower latitudes, then the electron events reappeared, only at somewhat reduced intensity. When the recurrent increases started to be accompanied by ~ 0.5 MeV protons, then the characteristic delay of the electron maximum from the proton maximum also reappeared, just as in the southern hemisphere (see Fig. 18, Simnett and Roelof, 1997). However, when Ulysses reached $\sim 30^\circ$ latitude, which was where in the southern hemisphere the increases of the electrons and the protons had simultaneous maxima, somewhat surprisingly the electron increases disappeared. The electron increase around day 149, 1996 was the last one where the electrons lagged the protons, and this was referred to as N6 in Roelof *et al.* (1997).

In Fig. 18 we compare the Ulysses 250–2000 MeV proton intensity observed in the northern hemisphere with that observed in the southern hemisphere. Note that in this figure time is running from left to right for the measurements in the southern hemisphere (lower curve) and from right to left for the measurements in the northern hemisphere (upper curve). At the top of the figure the radial distance and heliographic latitude are indicated for the Ulysses southern hemisphere passage. The northern pass is chosen such that the heliographic latitudes are approximately the same. The recurrent variations within the 2 1/2 years in the southern hemisphere are modulated on the time scale of one sidereal solar rotation. In the southern hemisphere the amplitude of the recurrent cosmic ray decreases had its maximum around 30°S and decreased towards both lower and higher latitudes; this is not observed in the northern hemisphere.

We presume that the driving force for the particle phenomena is the recurrent high-speed solar wind stream. Direct evidence for this vanished at Ulysses around 35° during the southern pass and reappeared just below 30° on the northern descent. The solar wind stream in the northern hemisphere (Fig. 17) is neither so uniform in intensity nor so regular in phase as it was in the south. This is reflected in phase changes in the galactic cosmic ray modulation. One very noticeable difference between the two hemispheres is the lack of relativistic electrons in the northern hemisphere. While this phenomenon is still under study, it seems likely that it is related to the absence of a strong and regular solar wind stream in 1996 and 1997.

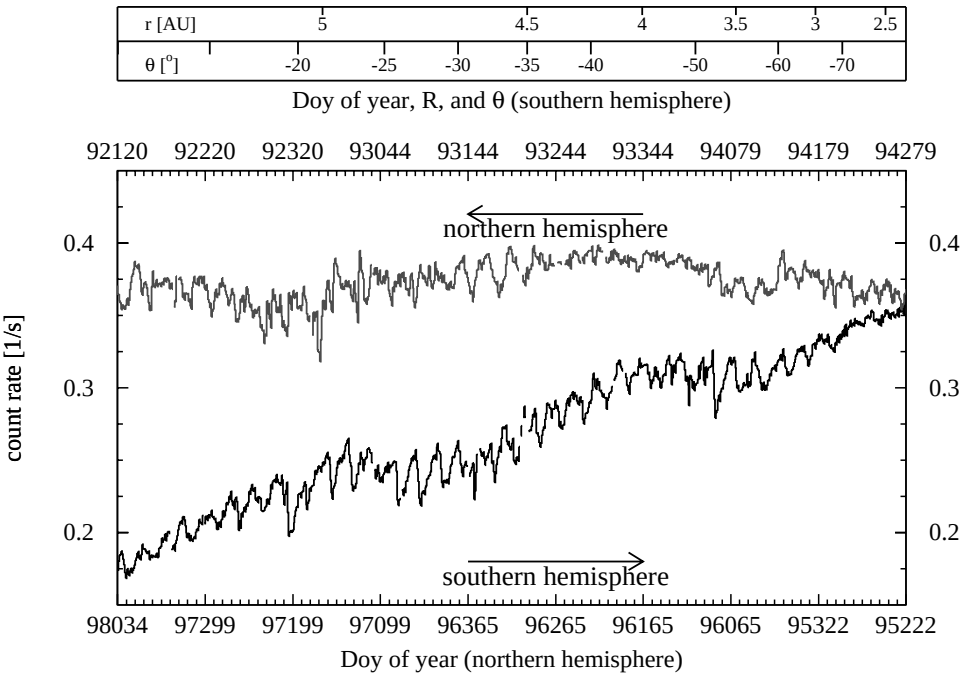

Figure 18. A comparison of the 250–2000 MeV proton intensity at Ulysses for the southern ascent from the equator to the 80° (upper time scale) and for the northern descent from 80° to the equator (lower time scale). Note: The period of the fast latitude scan in 1994/5 is not shown. The latitude and radial distance are shown at the top of the figure for the southern hemisphere; they are similar in the northern hemisphere.

4.3.1. *The Electron-Proton Delays*

The clue to the nature of the energetic particle acceleration processes occurring in the outer heliosphere came with the detection of delays between the intensity maxima of slow protons and fast electrons, with the electron maxima occurring later. An additional clue was the almost clock-like nature of the timing of the electron maxima in the southern hemisphere, when corrected for the position of Ulysses in heliocentric coordinates (Roelof *et al.*, 1996).

Figure 19 shows the data in more detail for 20 solar rotations, starting on 3 August 1996 and ending on 23 December 1997. This covered the Ulysses passage from a latitude of 31°N to the heliographic equator. Also shown in this figure as vertical bands are the times of forward (solid line) and reverse (dotted line) shocks (or waves) observed by the plasma and magnetic field instruments on Ulysses (Forsyth, personal communication). The purpose of this plot is to emphasize the relative timing of the particle events and the plasma signatures. After rotation N14 there is no electron event associated with either a forward or reverse shock or wave and the electron increases that are seen have some significant phase shifts with respect to our 26-day solar rotation cycle. This was discussed in more detail by

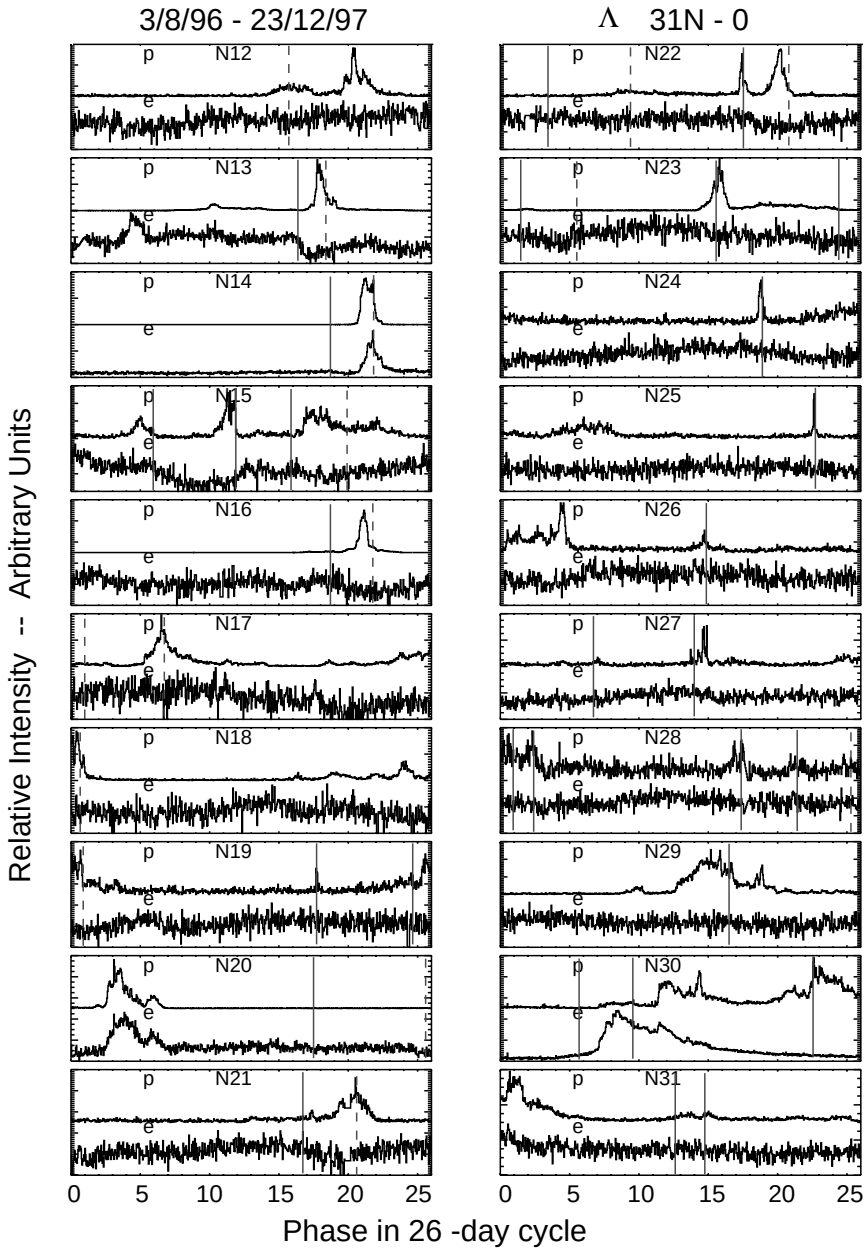

Figure 19. The relative timing of 53–107 keV electrons (e) and 0.48–0.96 MeV protons (p) seen during the Ulysses northern pass from 3 August 1996–23 December 1997. The data are plotted on a strict 26-day cycle, corresponding to a solar rotation, and the rotations are numbered N12-31 after the sequence started by Roelof *et al.* (1997). The vertical lines indicate times of forward (solid) and reverse (dotted) shocks seen at Ulysses. Λ is the heliographic latidude of Ulysses, and it goes from 31°N at the start of N12 to 0° by the end of N31.

Roelof *et al.* (1997). The electron increases are more readily associated with the reverse shock plasma signature than with the forward shock.

We believe that the differences between the southern and northern passes of Ulysses are a clue to the nature of the electron acceleration in CIRs. During the southern pass, the corotating stream was not only strong, but stable (Roelof *et al.*, 1996). However, in 1995 the modulation of the galactic cosmic rays was weak until early 1996, when Ulysses went below $\sim 50^\circ$ N. Figure 17 shows that this was true both at IMP 8 and at Ulysses. One feature of the southern hemisphere pass was that in the streamer belt below $|\Lambda| \sim 30^\circ$ the strongest proton events were associated with the forward-reverse shock pairs, with the maximum intensity seen around the time of the reverse shock. In the northern hemisphere there have not been so many reverse shocks. We draw attention to the forward-reverse shock pairs in rotations N14, N16, N21 and N22. These had significant proton increases below 1 MeV, but only N14 had any electrons associated with the shocks. Rotations N23–29 had protons associated with the forward shock (or wave) but no electrons above the background level.

Thus, for electrons to be accelerated it seems that we need a forward-reverse shock pair, plus an element of stability over at least several rotations of the corotating structure.

5. North-South Asymmetries in Modulation and 26-Day Variations

R. B. MCKIBBEN

Ulysses' fast latitude scan in 1994–95 provided a unique opportunity to study the latitude structure of modulation near solar minimum on a time scale ($\sim$1 year) short compared to the 11-year solar cycle. As reported by Simpson *et al.* (1996) and Heber *et al.* (1996), the modulated intensities of galactic cosmic rays and anomalous components were $\sim$10–20% higher over the north solar polar region than over equivalent latitudes in the south polar region. Furthermore, the latitude variation of the fluxes was symmetric about a surface 7–10 degrees south of the heliographic equator rather than about the equatorial plane itself. When analyzed with respect to a latitude of 10° S, the intensities of galactic cosmic rays and anomalous components were the same in the north and south at the same latitudinal separation from the southwardly displaced symmetry surface. Simpson *et al.* (1996) suggested that the flux excess over the north pole might be the result of the action of a constant latitude gradient over the more extended latitudinal range made available by the southward offset in the symmetry surface of modulation. The nature and cause of this southward offset in the symmetry surface of modulation has been the subject of much discussion. (See, for example, the discussion in Fisk *et al.*, 1998, pp. 191–192), and there is still no consensus on the explanation and implications of the observation. One simple explanation, a constant southward displacement of the equatorial current sheet, appears to be excluded by the observed near-constancy of the radial component of the interplanetary magnetic field observed during passage

from the south to the north polar regions in the fast latitude scan (Forsyth *et al.*, 1996).

Regardless of the existence and cause of the offset in the overall symmetry of the modulation, 26-day variations, presumably impressed by the CIRs near the ecliptic plane, were observed to the highest latitudes in both the north and south hemispheres. However, the variations were less prominent and more poorly organized near the north pole. This is more likely a temporal effect than a spatial effect related to the north-south asymmetry in modulation. During the fast latitude scan the inclination of the current sheet continued to decline towards the nearly flat inclination characteristic of solar minimum. Thus, the strength of the interaction between fast and slow wind near the ecliptic also continued to decline, so that any CIRs formed were weaker and developed at larger radii from the Sun. Consistent with this, Ulysses observed somewhat weaker 26-day variations in the cosmic ray intensity as it approached the equatorial band of slow solar wind after the north polar pass than it had observed during the initial climb to high latitude in 1993–1994. Thus there seems to be no clear, proven relationship between the observed North-South asymmetry in the global modulation and the strength of 26-day variations observed at high latitude.

6. Summary and Conclusions

H. KUNOW and M. A. LEE

Ulysses is the first spacecraft to explore the high-latitude range of the heliosphere. The discussion of corotating interaction regions at high latitudes in this chapter is therefore totally based on Ulysses observations. During its first orbit Ulysses observed a stable strong corotating interaction region from early 1992 through 1994 in the southern hemisphere. After a rapid latitude scan from south to north Ulysses observed only weaker CIRs from early 1996 to mid 1997 in the northern hemisphere.

We described the global structure of corotating interaction regions at high latitudes in Sect. 2 by discussing three model CIRs at fundamentally different latitudes. The most striking feature was the observation of CIR effects at latitudes well beyond the disappearance of the associated forward and reverse shocks up to the highest latitudes of 80°. Two different types of effects of CIRs upon energetic particles can be recognized: 1.) Observation of CIR-accelerated ions and electrons, and 2.) CIR-related periodic decreases of the galactic and anomalous cosmic ray component. The magnitude of both effects generally decreases with latitude, however, while the amplitude of accelerated ion events decreases by orders of magnitude, the latitude dependence for the modulation of galactic and anomalous cosmic rays and for accelerated electrons is much smaller. In addition, a time delay is observed between the maxima of accelerated ions and electrons that starts to show up at about 30°S and gradually increases up to $\sim$100 hours at 60°S.

All observational features are summarized in Sect. 2.3 together with the challenges they pose to theories and models. They indicate that particle transport between remote CIRs and the observer is a key to understanding effects of CIRs observed at high latitudes. In Sect. 3 we discussed possible models and their implications:

– Direct magnetic field connection across a large latitude range due to systematic field line weaving caused by solar differential rotation combined with an observed non-radial expansion of the solar wind was described in Sect. 3.1. Energetic particles propagate along these direct field line connections suffer adiabatic energy losses. The calculations in Sect. 2 show that the energy loss rate depends only on the initial position and velocity of the particles that favors faster electrons with much lower loss rates resulting in electron lagging low energy ions considerably. They have their maxima at about the same time as the recurrent decreases of galactic cosmic rays have their minima. Both electrons and GCRs have sufficiently high velocities to be able to connect to more distant portions of the reverse shock at high latitudes.

– An alternate phenomenon enabling latitudinal transport of energetic particles and cosmic rays to high latitudes is diffusion perpendicular to the average magnetic field due to random walk of field lines. This was discussed in Sect. 3.3.

In Sect. 4 we compared the observations of CIRs by Ulysses in the southern and northern heliosphere. CIRs are weaker in the northern hemisphere because the inclination of the streamer belt and the heliospheric current sheet (HCS) decreased with decreasing solar activity as Ulysses traveled to lower latitudes. In addition the warps of the current sheet are reduced in the northern hemisphere. The effects of CIRs on energetic particles are qualitatively similar in both hemispheres, however, much smaller in the northern hemisphere.

Section 4.3 described the variation of galactic cosmic rays during the northern CIR. The 26-day variation of galactic cosmic rays extended to the highest latitudes. A specific feature was the latitude dependence of galactic cosmic rays observed during the fast latitude scan in 1995. It was observed that the intensity increases symmetrically with increasing latitude if the plane of symmetry is at a latitude of $\sim 10^{\circ}$S instead of at the equator. The reason for this offset, however, currently cannot be explained.

While current models and theories predict many observations of CIRs at high latitudes, not all observed features can be explained by one of them alone. Since the effects discussed in Sect. 3 are probably all operating in the solar wind it will be necessary to develop a comprehensive theory which takes into account all effects and determines their relative importance depending on solar, local, and global conditions. This is discussed further in Sect. 5 of McKibben, Jokipii *et al.* (1999) in this volume.

Acknowledgements

We thank the International Space Science Institute for their hospitality during the 1998 CIR Workshop. Ulysses is a project of international cooperation between ESA and NASA. This work was supported in part by the German Space Agency DLR under contracts 50 ON 9106 and 9105, by NASA under Grants NAG 5-1479 and NAG 5-7097, and by the NSF Grant ATM-9633366. Other individual authors are funded by their National Agencies, *e.g.* NASA, and ESA. The research work of YQL has been supported in part by grants from U.S. National Science Foundation (ATM-9320357 and AST-9731623), National Aeronautics and Space Administration (Space Physics Theory and Supporting Research and Technology programs), and a SOHO/UVCS subcontract to the University of Chicago, and by the Visiting Scientist Program of the International Space Science Institute, Bern, Switzerland.

References

Balogh, A., Erdös, G., Forsyth, R. J., and Smith, E. J.: 1993, 'The Evolution of the Interplanetary Sector Structure in 1992', *Geophys. Res. Lett.* **20**, 2331–2334.

Balogh, A., Gonzalez-Esparza, J. A., Forsyth, R. J., Burton, M. E., Goldstein, B. E., Smith, E. J., and Bame, S. J.: 1995a, 'Interplanetary Shock Waves: Ulysses Observations in and out of the Ecliptic Plane', *Space Sci. Rev.* **72**, 171–180.

Balogh, A., Smith, E. J., Tsurutani, B. T., Southwood, D. J., Forsyth, R. J., and Horbury, T. S.: 1995b, 'The Heliospheric Magnetic Field over the South Polar Region of the Sun', *Science* **268**, 1007–1010.

Bame, S. J., Goldstein, B. E., Gosling, J. T., Harvey, J. W., McComas, D. J., Neugebauer, M., and Phillips, J. L.: 1993, 'Ulysses Observations of a Recurrent High Speed Solar Wind Stream and the Heliomagnetic Streamer Belt', *Geophys. Res. Lett.* **20**, 2323–2326.

Burlaga, L. F., Hundhausen, A. J., and Xue-pu Zhao: 1981, 'The Coronal and Interplanetary Current Sheet in Early 1976', *J. Geophys. Res.* **86**, 8,893–8,918.

Burton, M. E., Smith, E. J., Balogh, A., Forsyth, R. J., Bame, S. J., Philips, J. L., and Goldstein, B. E.: 1996, 'Ulysses Out-of-Ecliptic Observations of Interplanetary Shocks', *Astron. Astrophys.* **316**, 313–322.

Chandrasekhar, S.: 1961, *Hydrodynamic and Hydromagnetic Stability*, Dover Publications, New York.

Crooker, N. U., Gosling, J. T., Bothmer, V., Forsyth, R. J., Gazis, P. R., Hewish, A., Horbury, T. S., Intriligator, D. S., Jokipii, J. R., Kóta, J., Lazarus, A. J., Lee, M. A., Lucek, E., Marsch, E., Posner, A., Richardson, I. G., Roelof, E. C., Schmidt, J. M., Siscoe, G. L., Tsurutani, B. T., and Wimmer-Schweingruber, R. F.: 1999, 'CIR Morphology, Turbulence, Discontinuities, and Energetic Particles', *Space Sci. Rev.*, this volume, 179–220.

Desai, M. I., Marsden, R. G., Sanderson, T. R., Lario, D., Roelof, E. C., Simnett, G. M., Gosling, J. T., Balogh, A., and Forsyth, R. J.: 1999, 'Energy Spectra of 50-keV to 20-MeV Protons Accelerated at Corotating Interaction Regions at Ulysses', *J. Geophys. Res.* **104**, 6,705–6,719.

Fisk, L. A.: 1996, 'Motions of the Footpoints of Heliospheric Magnetic Field Lines at the Sun; Implications for Recurrent Energetic Particle Events at High Heliographic Latitudes', *J. Geophys. Res.* **101**, 15,547–15,553.

Fisk, L. A., Wenzel, K.-P., Balogh, A., Burger, R. A., Cummings, A. C., Evenson, P., Heber, B., Jokipii, J. R., Krainev, M. B., Kóta, J., Kunow, H., Le Roux, J. A., McDonald, F. B., McKibben, R. B., Potgieter, M. S., Simpson, J. A., Steenberg, C. D., Suess, S., Webber, W. R., Wibberenz, G., Zhang, M., Ferrando, P., Fuji, Z., Lockwood, J. A., Moraal, H., and Stone, E. C.: 1998, 'Global Processes that Determine Cosmic Ray Modulation – Report of Working Group 1', *Space Sci. Rev.* **83**, 179–214.

Fisk, L. A., and Jokipii, J. R.: 1999, 'Mechanisms for Latitudinal Transport of Energetic Particles in the Heliosphere', *Space Sci. Rev.*, this volume, 115–124.

Fisk, L. A., and Lee, M. A.: 1980, 'Shock Acceleration of Energetic Particles in Corotating Interaction Regions in the Solar Wind', *Astrophys. J.* **237**, 620–626.

Forsyth, R. J., Balogh, A., Horbury, T. S., Erdös, G., Smith, E. J., and Burton, M.: 1996, 'The Heliospheric Magnetic Field at Solar Minimum: Ulysses Observations from Pole to Pole', *Astron. Astrophys.* **316**, 287–295.

Forsyth, R. J., Balogh, A., Smith, E. J., and Gosling, J. T.: 1997, 'Ulysses Observations of the Northward Extension of the Heliospheric Current Sheet', *Geophys. Res. Lett.* **24**, 3101–3104.

Giacalone, J., and Jokipii, J. R.: 1997, 'Spatial Variation of Accelerated Pickup Ions at Corotating Interaction Regions', *Geophys. Res. Lett.* **24**, 1723–1726.

Gloeckler, G.: 1996, 'The Abundance of Atomic ^{1}H, ^{4}He and ^{3}He in the Local Interstellar Cloud from Pickup Ion Observations with SWICS on Ulysses' *Space Sci. Rev.* **78**, 335–346.

Gosling, J. T., Bame, S. J., McComas, D. J., Phillips, J. L., Pizzo, V. J., Goldstein, B. E., and Neugebauer, M.: 1993, 'Latitudinal Variations of Solar Wind Corotating Stream Interaction Regions: Ulysses', *Geophys. Res. Lett.* **20**, 2789–2792.

Gosling, J. T., Bame, S. J., McComas, D. J., Phillips, J. L., Pizzo, V. J., Goldstein, B. E., and Neugebauer, M.: 1995, 'Solar Wind Corotating Stream Interaction Regions out of the Ecliptic Plane: Ulysses', *Space Sci. Rev.* **72**, 99–104.

Gosling, J. T., Bame, S. J., Feldman, W. C., McComas, D. J., Riley, P., Goldstein, B. E., and Neugebauer, M.: 1997, 'The Northern Edge of the Band of Solar Wind Variability', *Geophys. Res. Lett.* **24**, 309–312.

Gosling, J. T., and Pizzo, V. J.: 1999, 'Formation and Evolution of CIRs and Their 3-D Structure', *Space Sci. Rev.*, this volume, 21–52.

Heber, B., Dröge, W., Kunow, H., Müller-Mellin, R., Wibberenz, G., Ferrando, P., Raviart, A., and Paizis, C.: 1996, 'Spatial Variation of $>$106 MeV Proton Fluxes Observed during the Ulysses Rapid Latitude Scan: Ulysses COSPIN/KET Results', *Geophys. Res. Lett.* **23**, 1513–1516.

Heber, B. Potgieter, M. S., and Ferrando, P.: 1997, 'Solar Modulation of Galactic Cosmic Rays: The 3D Heliosphere', *Adv. Space Res.* **19**, 795–804.

Heber, B., Sanderson, T. R., and Zhang, M.: 1999, 'Corotating Interaction Regions', *Adv. Space Res.*, in press.

Hoeksema, J. T., Wilcox, J. M., and Scherrer, P. H.: 1982, 'Structure of the Heliospheric Current Sheet in the Early Portion of Sunspot Cycle 21', *J. Geophys. Res.* **87**, 10,331–10,338.

Hoeksema, J. T., Wilcox, J. M., and Scherrer, P. H.: 1983, 'The Structure of the Heliospheric Current Sheet: 1978–1982', *J. Geophys. Res.* **88**, 9,910–9,918.

Hoeksema, J. T.: 1995: 'The Large-Scale Structure of the Heliospheric Current Sheet during the Ulysses Epoch', *Space Sci. Rev.* **72**, 137–148.

Hollweg, J. V., and Lee, M. A.: 1989, 'Slow Twists of Solar Magnetic Flux Tubes and the Polar Magnetic Field of the Sun', *Geophys. Res. Lett.* **16**, 919–922.

Isenberg, P. A.: 1997, 'A Hemispherical Model of Anisotropic Pickup Ions', *J. Geophys. Res.* **102**, 4,719–4,724.

Jokipii, J. R.: 1973, 'Radial Variation of Magnetic Fluctuations and Cosmic Ray Diffusion Tensor in the Solar Wind', *Astrophys. J.* **182**, 585–600.

Jokipii, J. R., and Thomas, B.: 1981, 'Effects of Drift on the Transport of Cosmic Rays - IV. Modulation by a Wavy Interplanetary Current Sheet', *Astrophys. J.* **243**, 1115–1122.

Jokipii, J. R., and Kóta, J.: 1989, 'The Polar Heliospheric Magnetic Field', *Geophys. Res. Lett.* **16**, 1–4.

Keppler, E., Fränz, M., Korth, A., Reuss, M. K., Blake, J. B., Seidel, R., Quenby, J. J., and Witte, M.: 1995, 'Observations of Energetic Particles with EPAC on Ulysses in Polar Latitudes of the Heliosphere', *Science* **268**, 1013–1016.

Kóta, J., and Jokipii, J. R.: 1995, 'Corotating Variations of Cosmic Rays near the South Heliospheric Pole', *Science* **268**, 1024–1025.

Kóta, J., and Jokipii, J. R.: 1997, 'Energy Changes of Particles Moving Along Field Lines', *25th Int. Cosmic Ray Conf. (Durban)* **1**, 213–216.

Kóta, J., and Jokipii, J. R.: 1998, 'Modeling of 3-D Corotating Cosmic Ray Structures in the Heliosphere', *Space Sci. Rev.* **83**, 137–145.

Kunow, H., Heber, B., Raviart, A., Paizis, C., Bothmer, V., Dröge, W., and Schmidt, J.: 1997, 'Time and Energy Dependence of 26-day Recurrent Decreases of $>$100 MeV Protons in the Inner Southern Heliosphere and its Correlation to Latitudinal Gradients: Ulysses COSPIN/KET Results', *25th Int. Cosmic Ray Conf. (Durban)* **1**, 381–384.

Lanzerotti, L. J., Armstrong, T. P., Gold, R. E., Maclennan, C. G., Roelof, E. C., Simnett, G. M., Thomson, D. J., Anderson, K. A., and Hawkins, S. E. III.: 1995, 'Over the Southern Solar Pole: Low-Energy Interplanetary Charged Particles', *Science* **268**, 1010–1013.

Lou, Y.-Q.: 1992, 'Three-Dimensional Magnetic Field Configurations in the Heliosphere', *J. Geophys. Res.* **97**, 17,183–17,188.

Lou, Y.-Q.: 1993, 'Propagation of Three-Dimensional Alfvén Waves and its Nonlinear Effects in the Solar Wind', *J. Geophys. Res.* **98**, 3,563–3,584.

Lou, Y.-Q.: 1994, 'Alfvénic Disturbances in the Equatorial Solar Wind with a Spiral Magnetic Field', *J. Geophys. Res.* **99**, 14,747–14,760.

Lou, Y.-Q.: 1996, 'Corotating Shock Accelerated Particles Guided by Wavy Spiral Magnetic Fields in the Solar Wind at High Heliographic Latitudes', *Geophys. Res. Lett.* **23**, 609–612.

McComas, D. J., Balogh, A., Bame, S. J., Barraclough, B. L., Feldman, W. C., Forsyth, R. J., Goldstein, B. E., Gosling, J. T., Funsten, H. O., Neugebauer, M., Riley, P., and Skoug, R.: 1998, 'Ulysses' Return to the Slow Solar Wind', *Geophys. Res. Lett.* **25**, 1–4.

McKibben, R. B., Jokipii, J. R., Burger, R. A., Heber, B., Kóta, J., McDonald, F. B., Paizis, C., Potgieter, M. S., and Richsrdson, I. G.: 1999, 'Modulation of Cosmic Rays and Anomalous Components by CIRs', *Space Sci. Rev.*, this volume, 307–326.

Northrop, T. G.: 1963, *The Adiabatic Motion of Charged Particles*, John Wiley, New York.

Ogilvie, K., and Roelof, E. C.: 1999, 'Energetic Ions and the Structure of Corotating Interaction Regions', *J. Geophys. Res.*, submitted.

Phillips, J. L., Balogh, A., Bame, S. J., Goldstein, B. E., Gosling, J. T., Hoeksema, J. T., McComas, D. J., Neugebauer, M., Sheeley Jr., N. R., and Wang, Y.-M.: 1994, 'Ulysses at 50° South: Constant Immersion in the High-Speed Solar Wind', *Geophys. Res. Lett.* **21**, 1105–1108.

Pizzo, V. J., and Gosling, J. T.: 1994, '3-D Simulation of High-Latitude Interaction Regions: Comparison with Ulysses Results', *Geophys. Res. Lett.* **18**, 2063–2066.

Reiner, M. J., Fainberg, J., and Stone, R. G.: 1995, 'Large-Scale Interplanetary Magnetic Field Configuration Revealed by Solar Radio Bursts', *Science* **270**, 461–464.

Roberts, D. A.: 1990, 'Turbulent Polar Heliospheric Fields', *Geophys. Res. Lett.* **17**, 567–570.

Roelof, E. C., Simnett, G. M., and Tappin, S. J.: 1996, 'The Regular Structure of Shock-Accelerated 40–100 keV Electrons in the High-Latitude Heliosphere', *Astron. Astrophys.* **316**, 481–486.

Roelof, E. C., Simnett, G. M., Decker, R. B., Lanzerotti, L. J., Maclennan, C. G., Armstrong, T. P., and Gold, R. E.: 1997, 'Reappearance of Recurrent Low-Energy Particle Events at Ulysses/HI-SCALE in the Northern Hemisphere', *J. Geophys. Res.* **102**, 11,251–11,262.

Sanderson, T. R., Marsden, R. G., Wenzel, K.-P., Balogh, A., Forsyth, R. J., Goldstein, B. E.: 1994, 'Ulysses High-Latitude Observations of Ions Accelerated by Corotating Interaction Regions', *Geophys. Res. Lett.* **21**, 1113–1116.

Sanderson, T. R., Marsden, R. G., Wenzel, K.-P., Balogh, A., and Forsyth, R. J.: 1995, 'High-latitude Observations of Energetic Ions during the First Ulysses Polar Pass', *Space Sci. Rev.* **72**, 291–296.

Sanderson, T. R., Bothmer, V., Marsden, R. G., Trattner, K. J., Wenzel, K.-P., Forsyth, R. J., and Goldstein, B. E.: 1996, 'Ulysses Observations of Energetic Ions over the South Pole of the Sun', D. Winterhalter *et al.* (eds.), *Solar Wind Eight*, AIP Conf. Proc., pp. 411–414.

Sanderson, T. R., Lario, D., Maksimovic, M., Marsden, R. G., Tranquille, C., Balogh, A., Forsyth, R. J., and Goldstein, B. E.: 1999, 'Current Sheet Control of Recurrent Particle Increases at 4–5 AU', *Geophys. Res. Lett.* **26**, 1785–1788.

Sayle, K. A., and Simnett, G. M.: 1998, 'High Latitude Ulysses Observations of CIR Accelerated Ions and Electrons', *Astron. Astrophys.* **331**, 405–410.

Schatten, K. H., Wilcox, J. M., and Ness, N. F.: 1969, 'A Model of Interplanetary and Coronal Magnetic Field, *Sol. Phys.* **6**, 442–455.

Schulz, M.: 1973, 'Interplanetary Sector Structure and the Heliomagnetic Equator', *Astrophys. and Space Sci.* **24**, 371–383.

Simnett, G. M., Sayle, K. A., Roelof, E. C., and Tappin, S. J.: 1994, 'Corotating Particle Enhancements out of the Ecliptic Plane', *Geophys. Res. Lett.* **21**, 1561–1564.

Simnett, G. M., Sayle, K. A., Tappin, S. J., and Roelof, E. C.: 1995a, 'Corotating Particle Enhancements out of the Ecliptic Plane', *Space Sci. Rev.* **72**, 327–330.

Simnett, G. M., Sayle, K. A., and Roelof, E. C.: 1995b, 'Differences between the 0.35–1.0 MeV/Nucleon H/He Ratio in Solar and Corotating Events at High Heliolatitude', *Geophys. Res. Lett.* **22**, 3365–3368.

Simnett, G. M., and Roelof, E. C.: 1997, 'Acceleration and Modulation of Energetic Particles in the 3-D Heliosphere by Corotating Interaction Regions', *Adv. Sp. Res.* **19**, 859–868.

Simnett, G. M., Kunow, H., Flückiger, E., Heber, B., Horbury, T., Kóta, J., Lazarus, A., Roelof, E. C., Simpson, J. A., and Zhang, M.: 1998, 'Corotating Particle Events', *Space Sci. Rev.* **83**, 215–258.

Simpson, J. A., Anglin, J. D., Bothmer, V., Connell, J. J., Ferrando, P., Heber, B., Kunow, H., Lopate, C., Marsden, R. G., McKibben, R. B., Müller-Mellin, R., Paizis, C., Rastoin, C., Raviart, A., Sanderson, T. R., Sierks, H., Trattner, K. J., Wenzel, K.-P., Wibberenz, G., and Zhang, M.: 1995, 'Cosmic Ray and Solar Particle Investigations over the South Polar Regions of the Sun', *Science* **268**, 1019–1023.

Simpson, J. A., Zhang, M., and Bame, S. J.: 1996, 'A Solar Polar North-South Asymmetry for Cosmic Ray Propagation in the Heliosphere: The Ulysses Pole to Pole Rapid Transit', *Astrophys. J. Lett.* **465**, L69–L72.

Siscoe, G. L., and Intriligator, D. S.: 1993, 'Three Views of Two Giant Streams – Aligned Observations at 1 AU, 4.6 AU, and 5.9 AU', *Geophys. Res. Lett.*, **20**, 2267–2270.

Skilling, J.: 1971, 'Cosmic Rays in the Galaxy: Convection or Diffusion ?', *Astrophys. J.* **170**, 265–273.

Smith, E. J., Neugebauer, M., Balogh, A., Bame, S. J., Erdös, G., Forsyth, R. J., Goldstein, B. E., Phillips, J. L., and Tsurutani, B. T.: 1993, 'Disappearance of the Heliospheric Sector Structure at Ulysses', *Geophys. Res. Lett.* **20**, 2327–2330.

Wang, Y.-M., Sheeley Jr., N. R., Phillips, J. L., and Goldstein, B. E.: 1997, 'Solar Wind Stream Interactions and the Wind Speed - Expansion Factor Relationship', *Astrophys. J. Lett.* **488**, L51–L54.

Wilcox, J. M., and Ness, N. F.: 1965, 'Quasi-Stationary Corotating Structure in the Interplanetary Medium', *J. Geophys. Res.* **70**, 5,793–5,805.

Wimmer-Schweingruber, R. F., von Steiger, R. and Paerli, R.: 1997, 'Solar Wind Stream Interfaces in Corotating Interaction Regions: SWICS/Ulysses Results', *J. Geophys. Res.* **102**, 17,407–17,417.

Zhang, M.: 1997, 'A Linear Relationship between the Latitude Gradient and 26-day Recurrent Variation in the Fluxes of Galactic Cosmic Rays and Anomalous Nuclear Components - I. Observations', *Astrophys. J.* **488**, 841–853.

Zurbuchen, T. H., Schwadron, N. A., and Fisk, L. A.: 1997, 'Direct Observational Evidence for a Heliospheric Magnetic Field with Large Excursions in Latitude', *J. Geophys. Res.* **102**, 24,175–24,181.

Zurbuchen, T. H., Fisk, L. A., Schwadron, N. A., and Pizzo, V.: 1999, 'A Simple Model for the New Heliospheric Field Configuration and the High-Latitude Transport of Low-energy Particles', *J. Geophys. Res.*, in press.

Address for Offprints: H. Kunow, Institut für Experimentelle und Angewandte Physik, Universität Kiel, Leibnizstr. 11–19, D–24118 Kiel, Germany